Clinical Relevance of Immune Cells in Pancreatic Adenocarcinoma and their Implication in Immunotherapy

Thesis

CLINICAL RELEVANCE OF IMMUNE CELLS IN PANCREATIC ADENOCARCINOMA AND THEIR IMPLICATION IN IMMUNOTHERAPY

Thesis submitted by

Giovanni Francesco Castino

IRCCS - Humanitas Research Hospital - Rozzano (MI), Italy

Affiliated Research Centre to “The Open University” Milton Keynes, UK

For the degree of Doctor of Philosophy

International PhD programme in Immunology and Immunopathology

Under the supervision of:

Director of studies: Dr. Federica Marchesi

Supervisor: Dr. Paola Allavena

External Supervisor: Prof. Philipp Beckhove

23 January 2018

Abstract

This thesis summarizes the work I have done during my PhD training, focused on the immune microenvironment of pancreatic adenocarcinoma (PDAC). The aim was to delineate key features of immunologic and tumour components shaping the biology of pancreatic cancer. Immunotherapy has been largely explored as a promising anticancer approach but not convincingly introduced yet for this tumour type. The results here summarized could contribute to a better understanding of the microenvironment of human PDAC and foster the introduction of immunotherapeutic strategies into the clinical practice.

The first section of the thesis summarizes the work done to investigate the occurrence of tertiary lymphoid tissue (TLT) in PDAC. TLT has been demonstrated to coordinate the recruitment and activation of adaptive immune cells in several tumour settings. This work documents the occurrence of TLT in pancreatic cancer, addresses the prognostic role of B cells according to their spatial distribution within TLT and tests the hypothesis that TLT can serve as immunological sites that contribute to efficacy of immunotherapeutic vaccination.

The second section is focused on the intersection between cancer metabolism and immune function in PDAC. In order to unearth early metabolic alterations in PDAC, we have analyzed the pancreatic juice, a relatively unexplored liquid biopsy potentially enriched with tumor-derived metabolites. Our results indicate a specific metabolic signature that allows to single out PDAC from other pancreatic pathologies and reveal an important link between glucose metabolism and accumulation of PD-1^{+} cells in PDAC tumors.

Table of contents

INTRODUCTION

1. Immune infiltrate of solid tumours

1.1 Introduction

The tumour microenvironment refers to the site wherein tumour cells interact with surrounding or recruited host cells. It is established in literature that these interactions are strongly related to an inflammatory condition, given by the intrinsic ability of the tumour mass to recruit immune and inflammatory cells [1].

The role of the tumour microenvironment has been closely investigated in the last decades, and so far it has been considered of primary importance for the evolution of the disease. In light of recent knowledge, tumour-infiltrating leukocytes are potentially able to exert both pro- and anti-tumour functions. Generally, the tumour microenvironment is largely infiltrated by adaptive and innate immune cells, and it has been demonstrated that both compartments can either sustain tumour development or mediate its rejection, depending on their phenotype [2-5].

In this first part of the introduction, I will give an overview of the variety of immune cells that populate the tumour microenvironment.

1.2 Innate immune cells and cancer-related inflammation

The paradoxical pro-tumour behaviour of innate immune cells can be ascribed to the opposite actions that these cells have to fulfil during the inflammatory response. During inflammation, innate immune cells have to support the adaptive immune system to specifically target infectious agents, and on the other side, the same cells are also involved in the wound-healing process required for the recovery from the damage induced by inflammation, supporting thus angiogenesis, tissue remodelling, and secretion of epithelial or stromal growth factors [2-4, 6, 7]. Neoplastic cells can subvert the intrinsic plasticity of innate immune cells in a double-edged sword manner, exploiting such wound-healing functions to sustain cancer neo-genesis and progression.

Inflammation is an immune-mediated response that spontaneously occurs during cancer development. Cancer-related inflammation, mainly promoted by the innate immune system, affects the tumorigenic process modulating cellular proliferation, rate of mutagenesis, and angiogenesis [2-4]. Accordingly, it has been reported that 15-20% of human cancers are associated to a chronic inflammatory condition. Helicobacter Pylori, Papilloma virus, and Hepatitis B or C virus infections are considered risk factors for gastric cancer, cervical cancer and hepatocellular carcinoma respectively [2-4].

Inflammation has been recognized as an important factor in enhancing cancer occurrence, and it has been recently integrated as a new 'hallmark of cancer' [1]. Essentially, inflammatory cells sustain incipient neoplasia in the acquirement of hallmark capabilities by limiting cell death, through secretion of growth and survival factors, by affecting neovascularization processes, and by sustaining metastatic progression, with the activation of EMT programs and secreting extracellular matrix-modifying enzymes.

1.3 Adaptive immune cells

Seminal studies have been conducted elucidating the role of adaptive immune cells in the anti-tumour response, focusing almost exclusively on T lymphocytes [4, 8]. Wide international efforts have shown a clear association between the density of tumour infiltrating lymphocytes (TILs) and patient prognosis in different types of tumours [9]. It is indeed well accepted that tumour infiltrating T cells, namely CD4 or CD8 expressing cells, are major players in immune mediated anti-tumour response. Both of them have essential roles in limiting tumour incidence and controlling the growth of already established tumours, through either cytokine secretion (CD4 or helper T cells), or mediating direct tumour cell killing (CD8 or cytotoxic T cells) [10]. Evidence has been produced demonstrating an increased incidence of neoplastic diseases in immunocompromised conditions, such as in *Rag2*$^{-/-}$ mice (i.e. mice lacking adaptive immune cells) [8] or, more specifically, in mice with impaired T and NK cell functions [11-13]. These works underline the fundamental role of adaptive immune cells in controlling tumour incidence and progression, with particular attention to major pathways involved, such as the production of cytotoxic molecules (Perforin), inflammatory cytokines (IFN-γ), and the interaction of immunoregulatory receptors/ligands (Fas/Fas-L). Similar evidence, of increased cancer incidence in immunocompromised individuals, has been reported also in patients affected by acquired immunodeficiencies primarily involving the adaptive branch of the immune system [14-16]. This data confirms a major role for adaptive immune cells, and particularly T cells, in the tumour context. The antigen-specific antitumor function of CD8 and CD4 T cells has been exploited in conceiving novel antitumor therapies, namely immunotherapies, that produce antitumor effects by stimulating immune cells. Within immunotherapies, most promising are those that exploit T cell-mediated tumour control. I will discuss such approaches in paragraph **1.5** of this section. The other major component of tumour infiltrating adaptive immune cells is represented by B cells. Despite their biological relevance and high frequency in the tumour microenvironment,

B cells have been far less studied in cancer setting. Currently, in other pathological conditions such as in preclinical models of autoimmunity and transplantation, evidence has been produced pointing to the central role of B cells in coordinating T cell responses [17-19]. B lymphocytes can sustain the immune response producing cytokines/chemokines, such as IFN-γ, IL-12 and TNF-α [20] or by activation of T cells acting as professional antigen presenting cells (APC) [21]. On this last point, it has been demonstrated that B cells are fully equipped to activate CD4 T cells by expression of various co-stimulatory proteins (CD80, CD86, and CD40) and MHC-II (major histocompatibility complex-class II) molecules, but also CD8 T cells, through a mechanism known as cross-presentation of extracellular antigens on MHC-I [22-24]. It has been also hypothesized that in the tumour microenvironment, B cells could be even superior as APC than dendritic cells (generally considered the most efficient APC) [25, 26]. In fact, within the tumour tissue, B cells are the most frequent cell type able to perform cross-presentation of antigens [25, 26] and more importantly, they can accumulate rare antigens by high-affinity membrane bound immunoglobulins [27]. Finally, B cells are suited to act directly within tissues, by activating cytotoxic pathways, or by production of antibodies [28]. Although B cells are biologically able to initiate and mediate an effective antitumor immune response, their role in human solid tumours is still debated. In ovarian cancer, non-small cell lung carcinoma and cervical cancer, B cell infiltration was associated with improved survival and lower metastasis incidence [23, 29, 30]. However, other studies report that antibody secreting CD138+ B cells are associated to poor prognosis in epithelial ovarian cancer [31]. In the same study the production of tumour-specific antibodies was associated to late stage disease in 50% of patients [31].

Data regarding the dichotomy of B cell role in human cancer are scant and controversial, nonetheless it could open the way to the reappraisal of B cell function in tumours and foster efforts towards novel therapeutic interventions [32]. Beside a detailed characterization of B

cell phenotype and a deeper knowledge of the immune pathways that B lymphocytes can activate in the anticancer response, their localization in the tumour microenvironment is equally gaining a lot of importance. In fact, as illustrated in the next paragraph and in the first part of this thesis, B cells display distinct patterns of distribution in the tumour microenvironment, and their role in those topological localization is likely to be functionally different [33].

1.4 Tertiary Lymphoid Tissue

Effective anti-tumour immune responses are generated by cellular interactions occurring in the context of lymphoid organs. Recently, experimental and clinical studies have suggested that this oversimplified model could not be exclusive. Robust evidence indicates that during the course of chronic inflammatory or infectious reactions, initiation of adaptive immune responses and priming of naïve T cells can occasionally occur extra-nodally, in peripheral tissues, within structures defined as tertiary lymphoid tissue or structures (TLT, or TLS) [34-39]. Tertiary lymphoid tissue is a well-defined topological and immunological compartment, capable of sustaining the recruitment of lymphocytes from the blood [40-42] and potentially behaving as a functional immune site involved in the generation of adaptive immune responses. The occurrence of TLT in tumour tissues has recently begun to be documented, providing evidence of an important role of TLT in the organization of immune response in cancer.

The specialized microarchitecture of TLT suggests that it could serve important immune functions, including the organization of B cell and T cell responses, clonal expansion, antibody generation, and immunoglobulin class switching. For these reasons, TLT occurrence and function in pathological conditions are now being deeply investigated. The general consensus is that in certain pathological conditions, such as autoimmune diseases and chronic infections, the presence of a lymphoid site could support disease progression,

acting as an alternative site for (self-)reactive lymphocyte recruitment and activation [38, 43-45]. Given its role in initiating and sustaining an antigen specific immune response, TLT could “protect” the organism by restraining pathological insults, as in the case of infectious diseases. In particular, over the last years, the possibility that functional ectopic lymphoid tissue generates an efficient immune response in tumours has propelled research towards the definition of its occurrence in the tumour microenvironment, with the attractive perspective of identifying novel targets for immunotherapeutic approaches.

The literature available on the occurrence of TLT in the tumour microenvironment has grown in the last years and evidence has been provided that the aggregation of lymphocytes into architecturally organized structures is an important immune feature that should not be ignored. The presence of TLT has been documented in many tumours [37, 46], including lung [47], melanoma [48], colon [41, 49, 50], breast [51]. However, not every patient with a specific type of cancer develops TLT and, when it is present, its density, level of organization and contribution to disease varies considerably. TLT develops more frequently in some tumour types than in others, suggesting that certain tumours provide a microenvironment that appears as a permissive milieu for lymphoid neo-genesis [52].

The emerging evidence that adaptive immune responses can be triggered independently of secondary lymphoid organs is encouraging to deepen the general knowledge of TLT. The presence of TLT in tumours could represent an ectopic immune site for tumour antigen presentation and lymphocyte activation to take place. On the other hand, the pro-tumour role of chronic inflammation suggests that TLT may also represent a source of growth factors and pro-angiogenetic factors that sustains tumour progression [53]. Moreover, lymphatic vessels associated to TLT may provide an additional way for cancer cells to metastasize.

Due to the inability of cancer preclinical models to recapitulate the chronic inflammatory microenvironment of human cancer, murine models of TLT neo-genesis in cancer settings have not been generated so far. Therefore, the most suitable approach so far to study the

role of TLT in cancer has been to investigate its occurrence in large cohorts of patients and analyse its prognostic value as reported by M. C. Dieu-Nosjean et al. [37] (**Table 1** adapted from [37]).

The evaluation of TLT in the tumour microenvironment as a novel biomarker of antitumor response has been an important objective of my project.

Primary or metastasic tumors	Cancer types	Markers quantified within lymphoid aggregates by immunochemistry	Gene signature associated with TLS presence	Studied cases	Stages of the disease	Prognostic value
Primary tumors	Breast carcinoma	$FoxP3^+$ cells	ND	191 patients	Stage II to III	Negative
		$PNAd^+$ HEV	ND	146 patients	Stage I to III	Positive
		ND	Tfh, Th1, and CXCL13 gene expression	70 patients	Stage I to III	Positive
		DC-$Lamp^+$ mature DC	ND	146 patients	Stage I to III	Positive
	Colorectal carcinoma	$CD3^+$ T cells and $CD83^+$ mature DC	ND	40 patients	Stage I to IV	Positive
		ND	12-Chemokine gene signature	21 patients	Stage 0 to IVA	Positive
		DC-$Lamp^+$ mature DC	ND	25 patients	ND	Positive
		ND	CXCL13 and CD20 gene expression	125 patients	Stage I to IV	Positive
		$CD3^+$ T cells	ND	351 patients	Stage II to III	Positive
		Lymphoid follicles	ND	350 patients	Stage I to IV	Positive
	Lung carcinoma	DC-$Lamp^+$ mature DC	ND	74 patients	Stage I to II	Positive
		DC-$Lamp^+$ mature DC	ND	362 patients	Stage I to IV	Positive
		DC-$Lamp^+$ mature DC and $CD20^+$follicular B cells	ND	74 patients and 122 patients	Stage I to II and Stage III	Positive
	Melanoma	DC-$Lamp^+$ mature DC	ND	82 patients	Stage IA to IIIA	Positive
		ND	12-Chemokine gene signature	21 patients	Stage IV	Positive
Metastatic tumors	Renal cell carcinoma	DC-$Lamp^+$ mature DC	ND	52 patients	ND	Negative
	Colorectal carcinoma	DC-$Lamp^+$ mature DC	ND	70 patients	ND	Positive
		DC-$Lamp^+$ mature DC	ND	140 patients	ND	Positive

Table 1. Evaluation of TLT clinical relevance in solid tumours.

1.5 Immunotherapy in solid tumours

Research on cancer immunology is moving from the mechanistic comprehension of immune cell behaviour in the tumour microenvironment, to the translation of such knowledge to the clinical practice. Novel immunotherapeutic strategies have the aim to commit the immune system to exert its fight against cancer, by directly boosting the immune response or by reverting the immunosuppressive microenvironment [54]. The ability of the immune system to control tumour growth has been the subject of intense debate in the last century [55]. Here I will provide an overview of the approaches used so far to develop effective immunotherapeutic agents. Immunostimulating cytokines, such as GM-CSF, IL-2 and IFNα have been widely tested in different clinical trials, in order to boost immune cells recruitment to the tumour site, and sustain their effector functions [55-57]. Such immunotherapies have been successfully applied in clinical practice, but their therapeutic effect is limited in duration and restricted to few tumour conditions. Moreover, this strategy relies on the recruitment and stimulation of a wide range of immune cells subtypes, leading to important side effects that curbed the use of such immunostimulatory agents in clinical practice [58-60]. Beside the non-specific immune cell recruitment mediated by systemic administration of immunostimulatory cytokines, other strategies act by boosting antigen-specific immune responses. From this perspective, tumour vaccines are treatments that stimulate adaptive immune cells against known tumour antigens, by the direct administration of tumour peptides (peptide-based vaccines) [61], by the infusion of APC previously exposed to tumour antigens (mainly dendritic cell-based vaccines) [62], or by administration of autologous tumor-specific effector cells (adoptive cell transfer, ACT) [63]. More recently, the attention in the onco-immunology field has been catalysed by the encouraging results obtained with the FDA-approved checkpoint inhibitor therapies. Immunotherapeutic approaches with checkpoint inhibitors are based on antagonistic antibodies directed against immunosuppressive receptors (immune checkpoint) expressed on tumour infiltrating

leukocytes. Such treatments prevent immune cells in the tumour microenvironment from the otherwise frequent activation of inhibitory checkpoints. The PD1 receptor, expressed by T cells, and its ligands PD-L1/L2, expressed by tumour as well as other cells, constitute a predominant immune checkpoint axis operating in the tumour context. In the last few years, antibodies inhibiting the PD1 receptor or its ligands have been the most attractive immunotherapeutic strategy among checkpoint inhibitors [64]. In light of striking results in terms of disease remission in the clinical setting, the FDA has approved therapies based on antibodies targeting the PD1-PDL1 axis for the treatment of melanoma, lung cancer, and renal cell carcinoma [65-67].

Despite invaluable outcomes reached by checkpoint inhibitor treatments, a considerable proportion of not-responding patients is still documented in most clinical trials. The ever-growing knowledge of immune checkpoint pathways will provide further biomarkers for pre-treatment prediction and on-treatment evaluation of patients' response.

1.6 Immune biomarkers

The dynamic equilibrium of pro- and anti-tumour immune networks differs along stages and types of tumour disease, and increasing literature points to the immune infiltrate as a novel and appealing parameter for tumour staging and classification [68, 69]. However, the identification of tumour-specific immune profiles as well as the design of effective immunotherapeutic settings are challenged by the intrinsic heterogeneity of solid tumours. The function and prognostic relevance of tumour-infiltrating immune cells can vary according to the organ of origin and/or the stage of disease, and critically contributes to the complexity of the cancer microenvironment [70-72].

The current TNM staging system focuses primarily on tumour cells and views tumour progression as a cell-autonomous process without considering the host immune response [68-70]. It is based only on tumour invasion parameters, provides limited prognostic

information and does not predict response to therapy. In some patients, advanced-stage cancer can be stable for years, and, although rare, partial or full regression of metastatic tumours can occur spontaneously [9].

Given the limitations of the TNM system and the important value of immune cells, new systemic and local immunological biomarkers can represent a significant innovative strategy in the prediction of outcome and response to therapy. Evidence demonstrating the impact of immune-classification in several human cancers is always growing. Immune classification has a prognostic value that may strengthen the value of the TNM classification, providing more information and facilitating clinical decision. As mentioned already, immune infiltrate is heterogeneous among tumour types, and is different from patient to patient. Compared to earlier studies assessing the relevance of tumour-infiltrating lymphocytes (TILs) in human cancer, current approaches have been ameliorated by integrating the analysis of adaptive cells with the definition of specific subsets and their quantitative distribution in the tumour microenvironment. The analysis of location, density and functional orientation of different immune cell populations is named “immune contexture” [69]. The clinical translation of the studies demonstrating the prognostic value of the immune contexture in primary tumours has led to the definition of an Immunoscore, a grading of tumours based on immune-histological features [70].

Histo-pathological analyses of tumours have shown that the immune infiltrate is not randomly distributed: TILs are found within dense infiltrates in the centre of the tumour (CT), at the invasive margin (IM) of tumour nests and in stromal tertiary lymphoid tissue (TLT) [73]. In particular, the spatial aggregation of immune cells occupies a critical position in dictating patient outcome, as I will show in the first part of my thesis.

In summary, evaluation of the histo-pathological immune reaction occurring in cancer may provide novel information on prognosis and might contribute to identify patient subgroups more likely to benefit from immunotherapy.

1.7 Immune infiltrate of pancreatic cancer

My PhD project has been focused on pancreatic cancer. In order to contextualize the role of tumour infiltrating immune cells and how they might contribute in improving both disease diagnosis and treatment, in this paragraph I will introduce pancreatic cancer and provide an overview of available literature regarding the immune infiltrate characterizing this pathology. Pancreatic cancer can be classified according to the histological features of tumour cells, allowing identification of several tumour types, each showing distinct clinical behaviour and genetic profile. Within pancreatic cancers, the most common histo-type is represented by pancreatic ductal adenocarcinoma (PDAC), accounting for greater than 85% of pancreatic neoplasms [74]. PDAC is the fourth leading cause of death, with a five-year survival rate of less than 8% and is only modestly responsive to anticancer therapies [75]. PDAC genetic models showed that the immune infiltrate is mainly composed of immunosuppressive cells since the very early phases of the disease [76]. This evidence has been confirmed in human studies, showing that alternatively activated macrophages [77] [78], myeloid derived suppressor cells [79] [80], and Treg cells [81] are dominant within PDAC microenvironment, while immune effector cells are present in low numbers or are poorly cytotoxic [82]. These observations supported clinical efforts aimed to target immune effector cell populations using immune-checkpoint blockade therapies [83] [84]. The presence of endogenous anti-tumour T cells strongly improved the efficacy of anti-tumour checkpoint immunotherapies, suggesting that modulation of the immune composition in PDAC, in particular T cells, may offer clinical benefit in controlling PDAC progression [85]. Moreover, PDAC is characterized by the formation of a dense fibrotic desmoplastic reaction, that has been reported to represent a barrier limiting the delivery of chemotherapy [86] [87] and possibly the access of immune cells [88]. The clinical relevance of the microenvironment regarding tumour progression and determining disease recurrence is supported by preliminary data

suggesting a correlation between poorer outcome and the presence of desmoplastic reaction as well as the composition/quantity of tumour infiltrating immune cells resulting in a weaker adaptive immune response in PDAC [89] [90]. Not surprisingly several attempts have been made to evaluate the prognostic significance of tumour-infiltrating leukocytes in a variety of human non-PDAC cancers at the level of genomics, transcriptomics and histology [5]. Prognostic significance of pronounced leukocyte infiltration has been shown to be of associated with increased survival [5].

It is generally accepted that PDAC microenvironment is immunosuppressive and thus effective antitumor immune response is dampened. In this scenario, immunotherapeutic approaches should be prompted at reverting the immunosuppressive mechanisms that dominate PDAC contexture, in order to redirect the dysfunctional immune microenvironment in an effective antitumor immune response.

2. Tumour Metabolism

2.1 Introduction

Recently, many efforts have been made on shedding light on the complex interconnection between cancer, immune cells and metabolism. Overall, metabolic reprogramming is a well-described event, and, in the tumour setting, it has been frequently documented as a feature of both cancer and infiltrating immune cells [1, 91]. The metabolic reprogramming occurring in cancer cells is currently investigated as a source of promising targets for novel therapeutic strategies. Moreover, a careful evaluation of the metabolic profile of cancer cells might pave the way to the discovery of biomarkers able to predict patients' prognosis and treatment responsiveness [92, 93]. On the immune side, the limited nutrient availability imposed by tumour cells determines a cascade of metabolic adaptations in tumour-infiltrating immune cells. In the last decades, metabolism has emerged as a key feature in implementing our knowledge on immune cell biology [94] and might constitute a promising source to ameliorate anticancer immunotherapies.

In this second part of the introduction, I will describe the main features of tumour metabolism, focusing on the possible implications for cancer immunotherapy. The effect of metabolic cues on immune cells infiltrating pancreatic cancer has been object of my studies and summarized in the second part of this thesis.

2.2 The Warburg Effect

Non-proliferating cells in normal tissues preferentially metabolize glucose to pyruvate and then, in order to maximize the production of ATP, they completely oxidize pyruvate into CO_2, in a process called oxidative phosphorylation (OXPHOS) [95]. OXPHOS requires oxygen to be engaged, and in conditions of normal availability of oxygen it is the principal pathway used by non-proliferating normal cells. However, in hypoxic conditions, OXPHOS is inhibited and ATP production is sustained by anaerobic glycolysis, a pathway that completely oxidizes pyruvate into lactate, producing far less ATP compared to OXPHOS. In contrast to what documented in normal non-proliferating cells, the physicist O. Warburg demonstrated that cancer cell metabolism relies primarily on glycolysis, even in normoxic conditions [96]. Since glycolysis is a pathway usually associated to hypoxia, its occurrence under normoxic conditions has been called aerobic glycolysis or Warburg effect.

As mentioned above, OXPHOS is more efficient than glycolysis in producing ATP, thus it is reasonable to suppose that ATP production is not the main purpose of glucose metabolism in cancer cells. It has been demonstrated that glycolysis is 100 times faster than OXPHOS [97], and this could result in a rapid modulation of energy production. Moreover, several intermediates of the glycolytic pathway are required for the biosynthesis of important constituents of cell organelles, such as lipids, nucleotides and amino acids. Given its role in both ATP production and biomass synthesis, glycolysis is preferred over OXPHOS by cancer cells [98]. In addition to highly proliferating neoplastic cells, activation of aerobic glycolysis characterizes almost all dividing cells, in order to meet their energetic and biosynthetic demands [99-101]. This includes embryonic progenitor cells, adult stem cells and activated immune cells.

Focusing on immune cells, the term immunometabolism refers to metabolic changes occurring in leukocytes during the effector phase of the immune response. In the last decades, much attention has been given to this peculiar feature of anti-tumour immune

responses, i.e. the key molecules and mechanisms driving the metabolic adaptation of immune cells occurring in this context [94, 102]. The metabolic reprogramming which characterizes the immune response to tumours is discussed below.

2.3 Metabolic reprogramming of immune cells in cancer

Upon activation, immune cells are metabolically reprogrammed to sustain massive proliferation and to mediate effector functions. Activated immune cells can adapt their metabolic requirements resembling characteristics of cancer cells, in order to fulfil their energetic demand, and to increase both biomass and effector molecule production [98]. Such modulation affects many of the known pathways involved in cell homeostasis, namely glycolysis, OXPHOS and fatty acid oxidation (FAO), depending on the cell type involved and on the context in which immune cell activation occurs. The dissection of the metabolic reprogramming that takes place in immune cells has been finely reviewed [94]. Here I will focus on effector T cells, which have been extensively characterized in several tumour settings, and display a clear role in mediating the anti-tumour immune response.

T cells undergo metabolic adaptation when raised against their cognate antigen. Since activated T cells share almost the same metabolic requirements with cancer cells, it has been postulated that a metabolic competition for nutrients might exist in the tumour microenvironment. One of the most elegant descriptions of such interplay has been recently addressed in a paper from Dr. Pearce's group, in which the authors demonstrated that not only the glucose metabolism of cancer cells profoundly impacts on tumour growth [103], but also that the enhanced glucose consumption of cancer cells restricts tumour infiltrating T cells, by inhibiting mTOR and glycolytic pathways and suppressing IFN-γ production. This suggests that tumour metabolism can promote cancer development by modulating antigen-specific immune response.

Another interesting aspect of the interplay between immune cells and tumour metabolism is represented by the immunomodulating role exerted by metabolites generated through the aberrant tumour metabolism, also referred to as oncometabolites [104-107]. Generally, soluble factors released by tumour cells have been reported to mediate immunosuppression, thus favouring the immunological escape frequently observed during cancer progression. An example of the immunomodulation mediated by oncometabolites is represented by the lactate released by cancer cells activating the Warburg effect. Lactate has been shown to critically affect activation and differentiation of myeloid cells, through induction of hypoxia-inducible factor 1 (HIF-1) signaling. Moreover, tumour-derived lactate blocks the activation of T cells, inhibiting the downstream activation of key transcription factors, hence impairing their effector functions [107], and contributes to extracellular pH lowering, affecting T cell survival signals [108].

Tumour metabolism is emerging as a critical regulator of the immune response. On the other hand, immunotherapy is rising as promising alternative to the conventional chemotherapeutic approach, albeit a significant proportion of patients do not respond to these treatments for still unknown reasons. The metabolic interplay between tumour and immune cells might provide the knowledge required for the development of combined therapies aimed at increasing immunotherapy effectiveness.

2.4 Targeting of metabolic pathways for cancer therapy

The altered tumour metabolism has been recognized as a specific hallmark of cancer [1]. Given its crucial role in determining cancer development and progression, tumour metabolism has been targeted by different approaches, as an alternative strategy to the more conventional chemotherapy. Classical antineoplastic drugs exert their anti-tumour functions essentially by targeting the enhanced proliferation typically associated with tumour cells. However, in many tumour settings chemotherapeutic drugs fail to restrict tumour

growth, due to intrinsic tumour resistance or to selection of resistant clones induced by the drug itself [109]. It is therefore essential to develop treatments to overcome the intrinsic or acquired tumour resistance to therapeutic treatments. To this purpose, tumour metabolism has emerged as a promising target, allowing for the generation of several inhibitors that selectively regulate altered metabolic pathways of cancer cells [110].

Numerous metabolic pathways have been successfully targeted in preclinical settings and have led to promising results. However, their translation into the clinical practice has been discontinuous. Beside the already discussed rationale of targeting glycolysis, other crucial bioenergetic and biosynthetic pathways have been considered in drug development [92]. For instance, nucleotide, amino acid and lipid biosynthesis can be suppressed in cancer cells, by developing selective inhibitors of rate-limiting enzymes. Oncometabolite production and secretion are other tumour-specific pathways that have been targeted in metabolism-targeted anti-tumour therapies. Of note, chemical inhibitors of the Monocarboxylate transporters MCT1 and MCT2 (involved in lactate uptake) and of MCT4 (responsible for lactate secretion) and lactate dehydrogenase (LDH) (the enzyme involved in lactate production) are in clinical or preclinical evaluation for cancer treatment [111, 112].

A relevant improvement in cancer treatment could be represented by combination therapies able to compensate the drawbacks of single therapies. Immunotherapies are experiencing an explosive growth; however, major concerns regarding the inter-patient variability, in terms of therapy response, have been raised [113]. Moreover, accurate prediction of response to therapy is still missing, meaning that other unknown factors are involved in determining immunotherapy responsiveness. To this end, the interplay between tumour metabolism and immune cells might result critical for the combination of metabolism-targeting therapies and immunotherapies [109].

In last decade the concept that also immune cells undergo metabolic adaptation during the phases of the immune response is emerging. Adaptive immune cells modify their metabolic

requirements during the differentiation process. Naïve T cells rely mostly on OXPHOS of fatty acids to produce ATP, and gradually switch toward a glycolytic phenotype when becoming effector T cells [114]. During the T cell activation phase, together with the differentiation in effector T cells, also a memory compartment is generated. Memory T cells exhibit an intermediate metabolic phenotype, characterized by OXPHOS, similarly to naïve cells, and a reduced glucose dependency compared to terminally differentiated effector T cells [115, 116]. The differentiation status of T cells has been reported to be crucial in a therapeutic prospective. Undifferentiated memory T cells show superior ability in conferring tumour protection in adoptive cell transfer settings [117, 118]. This has generated a growing interest in developing methods able to expand memory T cell subsets [119-122]. Such studies have effectively produced long-lived memory T cells by exposing naïve cells to homeostatic cytokines, by interrupting the normal differentiation process, or by regulation of the TCR signalling pathway. In addition, targeting the glycolytic pathway has been demonstrated to efficiently modulate the differentiation process of T cells. Enhancing glycolysis in activated CD8 T cells leads to the generation of terminally differentiated effector cells, while glycolysis inhibition favours the formation of long-lived memory T cells [123]. Deciphering the key factors that regulate T cell differentiation is mandatory to improve anti-tumour immunotherapeutic approaches. In this view, an accurate characterization of the metabolic requirements of immune cells in the tumour microenvironment could shed light on this fundamental aspect of T cell biology.

AIM of the STUDY

Pancreatic ductal adenocarcinoma (PDAC) is one of the most lethal cancers, characterized by a dismal survival. Conventional anticancer treatments are ineffective in controlling PDAC progression, posing the urgent need for novel therapeutic strategies. Immunotherapy has been largely explored as a promising anticancer approach but not convincingly introduced yet for this tumour type, and, furthermore, the comprehension of the mechanisms that lead to a successful immunotherapeutic strategy is still incomplete. In this thesis, the PDAC microenvironment has been thoroughly investigated, in order to delineate key features of immunologic and tumour components involved in the spontaneous anticancer immune response. These results could contribute to a better understanding of the microenvironment of human PDAC and foster the introduction in clinical practice of immunotherapeutic strategies in PDAC.

Tertiary lymphoid tissue (TLT) has been demonstrated to coordinate adaptive immune cell activation against cancer in several tumour settings. This thesis was designed to investigate TLT occurrence in PDAC, evaluating its role in cancer progression. Cancer cell metabolism has been recently demonstrated to influence tumour progression directly and by acting on tumour infiltrating immune cells (TILs). Here, the metabolism of pancreatic cancer cells has been investigated focusing on its impact on the phenotype and function of TILs.

METHODS

Patients and study design

The study included two Cohort of patients. Cohort 1 included 104 patients, aged older than 18 years, diagnosed with pancreatic ductal adenocarcinoma (PDAC) and who consecutively underwent surgery at the Humanitas Clinical and Research Centre, from February 2010 to December 2012. Clinicians prospectively assembled a clinical retrospective database by collecting patient demographics, clinical and histo-pathological data, as detailed in **Table 2**. Investigators who performed the assessment of immune variables were blinded to the clinical data. Patients with metastases at surgery (n=7) were excluded from the analysis. Detection of postsurgical local and distant tumour recurrences included a baseline thoracic and abdominal computed tomography (CT) and CA19-9 serum level evaluation. CT was repeated every 3 months during the first 2 years after surgery, and every 6 months afterward. CA19.9 assessment was repeated on a monthly basis during chemotherapy and concomitantly to CT scan afterward. As outcome variable we considered disease-specific survival (DSS), defined as any PDAC-related death detected in the observational period beginning immediately after surgery. Patients who died from causes other than PDAC were considered as lost to follow-up. The time of DSS was calculated from the date of surgery until date of death. The mean follow-up was 563.4 days (Standard Deviation=320.8 days). Cohort 2 comprised 40 patients aged older than 18 years, from which pancreatic juice was withdrawn during pancreasectomy. Patients were diagnosed postoperatively with pancreatic adenocarcinoma (n=31), pancreatitis (n=2), papillary tumours (n=4), neuroendocrine tumors (n=2), IPMN (n=1) (**Table 3**). Cohort 3 included 18 patients (**Table 4**)**.** Clinicians

prospectively assembled a clinical retrospective database by collecting patient demographics, clinical, and histopathological data, as detailed in **Tables 3** and **4.** All the patients were enrolled in the study after signed informed consent including collection of biological specimens and clinical data. The study was approved by the Ethical Committee of the Institution (protocol number ICH-595, approval issued on May 2009).

				CD20-TLT [a, b]		CD20-TILs[a, b]		CD8-TILs[a, b]	
		n	(%)	median	P	median	P	median	P
All cases		104	(100)	3.72		0.41		0.61	
Patient demographics									
Age (years)[c]		104	(100)	-	0,170	-	0.086	-	0.432
Gender	Female	54	(51.9)	3.90	Ref	0.38	Ref	0,61	Ref
	Male	50	(48.1)	3.35	0.464	0.44	0.686	0.60	0.502
Tumor features									
Nodal involvement	No	35	(33.6)	3.14	Ref	0,38	Ref	0,44	Ref
	Yes	67	(64.4)	4.31	0.857	0.45	0.325	0.64	0.187
Local Invasion	pT1-pT2	11	(10.6)	3.68	Ref	0,32	Ref	0,41	Ref
	pT3-pT4	91	(87.5)	4.02	0.431	0,43	0.456	0.61	0.375
Grade [d]	G1/ G2	47	(45.2)	4.17	Ref	0.38	Ref	0.57	Ref
	G3/ G4	44	(42.3)	3.53	0.351	0.47	0.816	0.64	0.930
Chemotherapy (CTX)									
Adjuvant	No	35	(33.7)	3.83	Ref	0.36	Ref	0.64	Ref
	Yes	69	(66.3)	3.56	0.937	0.43	0.575	0.57	0.310
Neo-Adjuvant	No	90	(86.5)	4.02	Ref	0.41	Ref	0.63	Ref
	Yes	14	(13.5)	2.01	0.200	0.42	0.848	0.39	0.287

Table 2. Summary of clinical and immunological variables of Cohort 1 patients. COX regression analysis (**a**). Densities as percent immune-reactive area at the tumor-stroma interface (**b**). Age was entered as continuous variable. dG1/G2, well-to moderately differentiated; G3, G4 poorly differentiated (**c**). R0, microscopic radical resection; R1, microscopic non-radical resection (**e**). “Ref” (reference): refers to the reference group used to calculate the p-value.

		N (%)
Patient Age	≤70 yrs	22 (55%)
	>70 yrs	18 (45%)
Patient Gender	Male	20 (50%)
	Female	20 (50%)
Diagnosis	Ductal	31 (77.5%)
	Adenocarcinoma	2 (5%)
	Pancreatitis	4 (10%)
	Papillary-Ampulla	2 (5%)
	Neuroendocrine	1 (2.5%)
	IPMN	
Tumour invasion*	pT1/pT2	11 (31%)
	pT3/pT4	25 (69%)
Nodal Status*	N0	10 (28%)
	N1	19 (53%)
	N2	5 (19%)
Tumour Grade*	G1/G2	24 (65%)
	G3/G4	13 (35%)

* Data refer only to tumour patients

Table 3. Summary of the clinical features relative to Cohort 2 patients.

		N (%)
Patient Age	≤70 yrs	14 (78%)
	>70 yrs	4 (22%)
Patient Gender	Male	9 (50%)
	Female	9 (50%)
Tumour invasion	pT1/pT2	0 (0%)
	pT3 /pT4	18 (100%)
Nodal Status	N0	4 (22%)
	N1	14 (78%)
	N2	0 (0%)
Tumour Grade	G1/G2	7 (39%)
	G3/G4	11 (61%)

Table 4. Summary of the clinical features relative to Cohort 3 patients.

Immunohistochemistry

2µm thick tissue slides from formalin processed and paraffin-embedded tumour sections were processed for immunohistochemistry. After deparaffinization and rehydration, sections were immersed in a water bath for antigen retrieval, and then incubated with 3% H2O2 for 15 minutes. Slides were autostained (IntelliPATH FLX, Biocare Medical) with primary antibodies raised against CD20 (DAKO, L26), CD8 (DAKO, C8/144B), CD68 (DAKO, KP1) and CD3 (DAKO, F7.2.38), or manually stained with antibodies against PD-1 (Abcam NAT105), DC-Lamp (Dendritics, 1010E1.01), PNAd (BD Pharmingen, MECA-79), Lyve-1 (Abcam, polyclonal), CXCL13 (R&D, polyclonal), CCL21 (R&D, polyclonal), Ki67 (DAKO, MIB-1), Bcl-6 (DAKO, PG-B6p), GLUT-1 (Abcam, clone EPR3015). This was followed by a 30-minute incubation with the DAKO Envision system (Dako) or Anti-Goat Polymer kit (Biocare). Brown colour was obtained using diaminobenzidine tetrahydrochloride (DAB) (Dako) as chromogen. Nuclei were lightly counterstained with a freshly made haematoxylin

solution (Medite). The sections were further washed in water, mounted and analysed under an optical microscopy.

Image analysis

After staining procedure, tissue sections were digitalized using a slide digital scanner (Olympus dotSlide). At least two independent operators blinded to any patient clinical data selected three non-overlapping and non-contiguous areas comprising of approximately 50% of tumour and 50% of stromal tissue and including $CD68^+$, $CD20^+$, $CD8^+$ or $PD1^+$ cells (**Figure IRA, A**). For CD20-TLT analysis, 3 non-contiguous fields were chosen representing the entire CD20 positive area within the TLT, regardless of the location in the tumour or in the stroma. When stained for CD20, TLT displayed a typical structure that can be recognized by operators.

Both sampled microscopic area and light density were maintained fixed throughout the analysis. Selected areas were quantified by computer-assisted image analysis, with ad hoc software, to obtain the percentage of immune reactive areas (IRA%) of the digitalized tissue surface (**Figure IRA, B-C**).

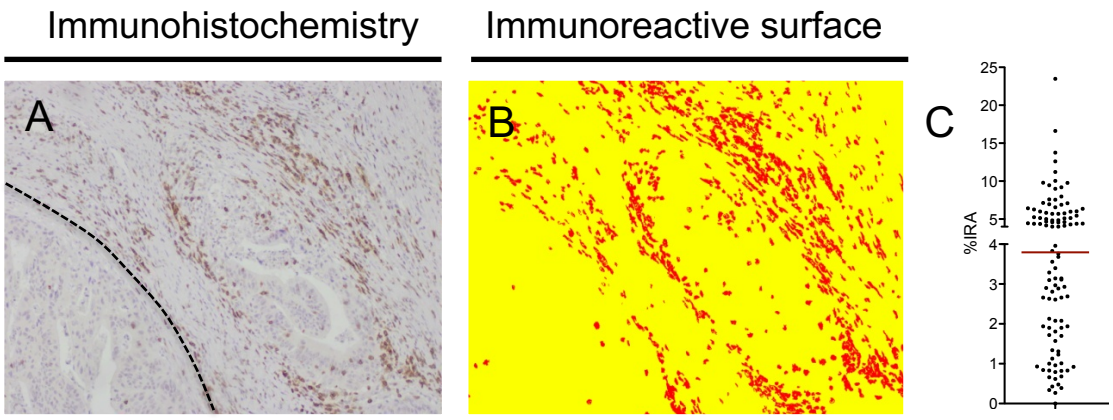

Figure IRA%. Computer-assisted image analysis workflow. Representative image of the three selected areas. Dashed line delimitates tumour tissue from stromal region (**A**). Discrimination of positive signal (red) from background signal (yellow) obtained by software analysis (**B**). Scatter dot-plot of IRA% values obtained from analysis of pictures; red line represents median (**C**).

The variable PD1-GC was expressed as a dichotomous value, assigning a positive value when PD1 positive cells were present in the germinal centre of previously assessed CD20-TLT. The extent of the overall distribution of CD20-TLT, CD20-TIL, CD8-TIL, CD68-TAMs, GLUT-1 and PD1-TILs IRA%, expressed as continuous variables, and PD1-GC score were used to perform statistical analyses. For each immune variable with continuous values (CD20-TLT, CD20-TILs, CD8-TILs), we stratified patients by grouping into quartiles.

Gene expression analysis

Patients were divided into TLT^{hi} (4th quartile n=5) and $TILs^{hi}$ (4th quartile n=5), according to CD20-TLT and CD20-TIL IRA% values and RNA was extracted from FFPE tissues using the RNeasy FFPE kit (QIAGEN); adjacent normal pancreatic tissue (n=5) was used as a control. RNA from Panc02 tumours was extracted after collagenase (Sigma Aldrich) digestion of tumour fragments and isolation of the leukocyte fraction by gradient centrifugation (Percoll (GE Healthcare life sciences)). Cells were re-suspended with PureZOL (Bio-Rad), and RNA was purified using RNeasy Plus Mini kit (QIAGEN) following manufacturer instructions. In each case, cDNA was obtained after an 8-cycle pre-amplification step, followed by reverse transcription with the RT^2 PreAMP cDNA synthesis kit (Qiagen). For $CD45^+$ cells from Panc02 murine models, pre-amplification step was not necessary, cells were isolated from anti-PD1 treated sh-PFK and sh-SCR tumors using the CD45 (TIL) MicroBeads, mouse kit (Miltenyi biotec). RNA was extracted with PureZOL (Bio-Rad), purified with RNeasy Plus Mini kit (QIAGEN) from both $CD45^+$ fraction and from CD45 negative flow through, and reverse transcription performed with the RT^2 cDNA synthesis kit (Qiagen). Real-Time PCR was performed using commercially available PCR Arrays (RT^2 ProfilerTM PCR Array System, Qiagen), on a ViiA™ 7 Real-Time PCR (Life Technologies). Differences in gene expression were analysed by the comparative threshold cycle (Ct) method with DataAssist™ (Life Technologies), after global normalization. Within PDAC

patients groups, samples with the lowest Ct variability (n=3) were selected for analysis. Hierarchical clustering was performed with the Cluster 3.0 software, including the whole gene-list available in the Array. The normalized signal value was adjusted to log transform data and “median” was selected to centre genes. Clustering was performed using the Pearson correlation function with Java TreeView and exported to heatmap images.

For the network analysis, uploading control and α–CD20-treated data set, containing gene identifiers and corresponding expression values, into the Ingenuity Pathways Analysis application generated significant pathways and molecular networks. The resulting Network Eligible molecules were overlaid onto a global molecular network based on the in Ingenuity’s Knowledge Base (Ingenuity® Systems, www.ingenuity.com), a uniquely structured repository of biological and chemical “findings” curated from various sources including the literature. The Functional Analysis of the network identified the biological functions most significant to the molecules in the network including the whole gene-list available in the Array.

PDAC murine models

All mice used for the orthotopic implantation of Panc02 cells were 8-week-old C57BL/6J females purchased from Charles River (Calco, Italy) and housed in a specific pathogen–free animal facility of the Humanitas Clinical and Research Centre, in individually ventilated cages. Procedures involving mice and their care were conformed to EU and Institutional Guidelines, and approved by the Italian Ministry of Health (project 5/2015). Murine Panc02 cell line was kindly provided by Dr. Piemonti (San Raffaele Hospital, Milan) and cultured in RPMI 1640 medium (Lonza) supplemented with 10% FBS, 2mM l-Glutamine. Cells were cultured in a humidified incubator with 5% CO_2, for one passage before *in vivo* injection. Mice were kept anesthetized during all surgical operation by intraperitoneal administration of a ketamine and xylazine solution. The stomach and the adherent pancreas were

exteriorized to expose the head of the pancreas, in which 30µl of 10^6 Panc02 cells suspension was injected using a 30-gauge insulin needle. All the organs were then returned to their original position and peritoneum and skin were sutured. Animals were randomized after surgery into two treatment groups, the first receiving 250µg of α–CD20 antibody (Genentech, clone 5D2), and the second receiving 250µg of the isotype-matched (IgG2a) irrelevant immunoglobulin (BioXCell C1.18.4), both by i.p. injection 3 days after surgery. After 3 weeks from surgery, mice were sacrificed and tumour masses collected. Single cell suspensions were obtained by incubating fragmented tumours with 0.5 mg/ml of clostridium histolyticum-derived collagenase (Sigma Aldrich) for 30 minutes at 37°C. Cells were then washed and tumour infiltrating leukocytes purified by a 44%/66% Percoll (GE Healthcare life sciences) gradient centrifugation. The purified leukocytes were washed and aliquoted for multi-colour FACS analysis or RNA extraction. Alternatively, tissues were fixed for immunohistochemical analysis.

Pancreatic cancer–prone LSL-$Kras^{G12D}$-Pdx1-Cre mice (KC mice) were bred, maintained and treated at the saprophytic and pathogen-free animal facility of the Molecular Biotechnologies Centre (Torino, Italy), as previously described [124]. Briefly KC mice were vaccinated at 32 weeks of age and every 3 weeks for a total of 3 rounds of vaccination. Vaccination was achieved by electroporation of femoral muscle with 50µg of plasmid (either mock pVAX vector or the human Enolase (ENO1) encoding vector). Mice of the same age were randomly assigned to control and treatment groups, and all groups were specifically treated concurrently. Mice were sacrificed 2 weeks after the last vaccination to perform histologic or immunohistochemical analyses. Splenocytes were analysed for the ability to secrete IFN-γ in response to the recombinant ENO1 ex vivo as described in [124]. Briefly, anti-IFN-γ capture mAb (mIFN-γ kit by BD) was used to coat nitrocellulose plates (Millipore, Milan, Italy) by overnight incubation at 4 °C. T cells from spleens were stimulated with rENO1 (10µg/ml), for 40 h at 37 °C and seeded at 3 x 10^5cells/well. All conditions were carried out

in quadruplicate. Plates were then analyzed following manufacturer' instructions using AEC (Sigma-Aldrich) substrate, and spots quantified with the microplate reader along with a computer-assisted image analysis system (AID, Amplifon, Milan, Italy). The number of spots was calculated by subtracting the number of spots in medium only (background) from that in the presence of stimuli.

Subcutaneous tumour models were obtained by injecting DT6606 or Panc02 cells. Murine DT6606 were derived from KC mice tumours and can be considered "early" tumour since they bear only one single mutation. Panc02 cells were originated from chemically induced tumour and harbor multiple mutations, therefore can be considered as a "late" lesion. Both cell lines were cultured in complete RPMI (RPMI 1640 medium (Lonza) supplemented with 10% FBS (Euroclone), 2mM l-Glutamine (Lonza), and 100 units of Potassium Penicillin and 100µg of Streptomycin Sulfate (Lonza) per 1ml of culture media). Cells were cultured in a humidified incubator with 5% CO2, for one passage before in vivo injection. Silenced cell lines sh-SCR and sh-PFK were generated as described in next paragraph of this section. Both cell lines were cultured in complete RPMI supplemented with Puromycin (Sigma Aldrich) 1µg/ml for two weeks before in vivo injection. For the immunotherapeutic protocol, animals were randomized after injection into two treatment groups, the first receiving 200µg of α–PD1 antibody (Bioxcell, clone RMP1-14), the second receiving 200µg of anti-trinitrophenol isotype control (Bioxcell, clone 2A3), both with i.p. injections starting 7 days after surgery, every 3 days. At 3 weeks from surgery, mice were sacrificed, and tumor masses collected for subsequent analysis. All tumour growth curves were generated by measuring tumour dimensions with caliper.

Lentiviral particles production and silencing validation

Plasmids encoding sh-RNA against murine *pfk-m* and scramble sequence (targeting a non-mammalian gene) were purchased from Sigma Aldrich (PFK-m: TRCN000012536;

Scramble: SHC002) as bacterial glycerol stocks. Both plasmids encode for Puromycin N-Acetyltransferase enzyme, which allowed the negative selection of transduced cells. Bacterial culture was established inoculating a small amount of the glycerol stock into 200ml LB (GE healthcare) supplemented with Ampicillin (Sigma Aldrich) 50μg/ml, and incubated overnight at 37°C under vigorous shaking. Plasmidic DNA was extracted using MAXI-Prep kit (Promega) following manufacturer's instructions.

Lentiviral particles were produced by co-transfection of 293T cell line using sh-RNA encoding plasmid together with packaging (ΔR8.2) and envelope (VSV-G) plasmids (both from Addgene). Supernatants containing lentiviral particles were collected 48 hours after transfections, and directly used on Panc02 cells to generate sh-SCR and sh-PFK cell lines. 1ml of supernatant was added to Panc02 cells cultured in 6-well plates when 50% of confluence was reached, and culture was immediately centrifuged at 300g for 1 hour. Then 2ml of fresh complete RPMI was added and cells incubated at 37°C overnight. Medium was replaced with fresh complete RPMI supplemented with 1μg/ml Puromycin (Sigma Aldrich) and maintained for two weeks before using cells in an *in vivo* experiment. During selection, mRNA was extracted from cells and tested to determine gene silencing of *pfk-m* as shown in graph **Fig. 4.8 B**.

Flow-cytometry

Absolute numbers of $CD19^+$, $CD3^+$, $CD11b^+$ cells were assessed by flow cytometry on peripheral blood leukocytes at day 0, 3, 7, 14 and 21 days from antibody injection. Trucount kit (BD Biosciences) was used to obtain absolute numbers. Tumor digests were analysed using the following fluorophore-conjugated primary antibodies: anti-CD45 (BD Pharmingen 30-F11), anti-CD19 (eBiosciences eBio1D3), anti-CD3 (eBiosciences 145-2C11), anti-CD11b (BioLegend M1/70), anti-CD8 (BioLegend 53-6.7), anti-PD1 (Biolegend, clone 29F.1A12). Zombie Aqua (Biolegend) amine-reactive fluorescent dye was used to perform

dead cell exclusion. 2-NDBG uptake was measured by incubating digested tumors in a 200μM 2-NBDG (Sigma Aldrich) solution (phosphate buffer saline, PBS) for 30 minutes at 37°C. Sample acquisition was performed on a BD LSRFORTESSA (BD Biosciences) and data analysed with FlowJo software.

Glucose uptake in vitro and image analysis

Panc02 and DT6606 cell lines were cultured in 48-well plate using complete RPMI until 70% confluence was reached. Cells were incubated in a 200μM 2-NBDG (Sigma Aldrich) solution (PBS) for 30 minutes at 37°C, washed and maintained in PBS during acquisition. Differential interference contrast (DIC) and fluorescent images were obtained with CellR wide field microscope (Olympus). Cells were seeded in three wells and a single wide field image per well was acquired (20X objective). DIC and FITC images were collected for each condition and analyzed using Fiji open-source software. Analysis was performed selecting single cells as region of interest (ROI) and measuring the mean fluorescent intensity (MFI) in FITC channel. At least 20 ROIs were measured in each well, and three wells were analyzed for both Panc02 and DT6606 cell lines.

Pancreatic juice collection and preparation

Pancreatic juice was collected intraoperatively in a vial containing anticoagulant and stored at 4°C until transportation to the laboratory for processing. Once in the laboratory, the sample was centrifuged within 5 hours of collection, aliquoted in EDTA-containing vials and stored at -80°C. Patients had been fasting overnight.

Nuclear magnetic resonance (NMR) spectroscopy

180μL of pancreatic juice were mixed with 20μL of D2O buffer (1.5M KH2PO4 dissolved in 99.9% D2O, pH 7.4, 2mM sodium azide and 0,1% 3-(trimethyl-silyl) propionic acid-d4

(TSP)). A total of 200μl of this mixture was transferred into a 3-mm NMR tube (Bruker BioSpin) for the analysis. NMR spectra of pancreatic juice samples were acquired using a Bruker IVDr 600MHz spectrometer (Bruker BioSpin) operating at 600.13MHz proton Larmor frequency, equipped with a 5mm PATXI H/C/N with 2H-decoupling probe including a z axis gradient coil, an automatic tuning-matching (ATM) and an automatic refrigerated sample changer (SampleJet). Temperature was regulated to 300 ± 0.1K with a BTO 2000 thermocouple.

Multivariate statistical analysis applied to metabolite quantification by NMR

All multivariate and univariate analyses regarding the NMR-based metabolomics study were performed by PLS_Toolbox 8.2.1 and homemade scripts, respectively, in Matlab 2016a programming environment. Metabolites signals deconvolution and integration was accomplished by an in-house developed software in MATLAB programming suited by Dr. P.G. Takis. The algorithm is based upon the unconstrained non-linear minimization (fitting) of the metabolite NMR signals, employing a combination of lorentzian-gaussian functions. By this approach, each NMR region of interest is decomposed and deconvoluted into its component parts, and then integrated to obtain the metabolite concentrations in arbitrary units. For the n x Fold concentration changes for each metabolite the following equation was employed:

$$n \times Fold = log_2\left(\frac{median\ of\ group\ 1}{median\ of\ group\ 2}\right)$$

Optical imaging

In vivo evaluation of glucose uptake was assessed using the fluorescent glucose analogue XenoLight RediJect 2-DG-750 probe (Perkin Elmer), following datasheet instructions. Imaging was performed *ex* vivo on excised tumors after 24 hours from i.v. injection of the

probe, using the IVIS Lumina III InVivo Imaging System (Perkin Elmer). The acquisition was performed using four filter pairs in order to calculate spectral unmixing. Emission was collected with a 790nm filter, while excitation was performed with four excitation filters (680, 700, 720, and 750nm). Binning value: 8; f/Stop: 2. Images were analyzed with Living Image 4.3.1 software (Perkin Elmer).

Statistical analysis

The associations between values of immune cells and other features concerning patient clinical conditions were estimated by Pearson simple linear regression analysis. A multivariate Cox proportional hazards model was developed to assess the role of immune variable density and demographic, clinical, and histo-pathologic features, in predicting the outcome of disease specific survival. Cox multivariate analysis was performed by entering variables with a P value lower than 0.05 at univariate analysis. Kaplan–Meier curves of DSS were plotted and the log-rank test was used to compare the curves of each subgroup of patients with pancreatic cancer. The use of quartiles as opposed to median is justified by the fact that prognostic effect of TLT was significant only for extremly low values of IRA% (1st quartile), whilst this was not the case for median values (data not shown). The second and third quartiles showed a trend towards a better prognosis, even if not significant, thus justifying their grouping with the fourth quartile. Biologically, this result suggests that TLT occurrence seems to be generally favourable, except for patients with very low density (1st quartile). The correlation between IRA% values of GLUT-1 and PD-1 were estimated by nonparametric Spearman Rank correlation coefficient test and linear regression analysis. Differences between groups were estimated by non-parametric Mann Whitney U test. When more than one variable was evaluated, two-way ANOVA test was used and P values calculated by Tukey's multiple comparisons post-test. In each experiment, sample size was at least 9 mice for each group. For each test, only two-sided P values lower than 0.05 were

considered statistically significant. All the analyses were done using SPSS (Version 22.0) and GraphPad Prism software (Version 4.1). To study the prognostic value of immune variables, we adhered to “Reporting Recommendations for Tumour Marker Prognostic Studies (REMARK)” [125] for high quality of tumour marker studies.

ACKNOWLEDGMENTS

The most part of this thesis has been performed by me during my four year PhD program. For some specific tasks I have taken advantage of helpful collaborations. Experiments in "Section **3**" have been carried out in collaboration with the group of Professor Franco Novelli (University of Turin). They have set up the experimental model of Eno1 vaccination, and provided us with data relative to the elispot-assay, and tissues from vaccinated and control KC mice.

Metabolomics profiling of pancreatic juice and the relative statistical analysis in "Section **4**" have been performed by Dr. Takis P. G. at Giotto Biotech s.r.l..

RESULTS

3. B cell duality in pancreatic cancer

3.1 Background and goal

In some tumour conditions, priming of antigen-specific T cells can occur extra-nodally in peripheral tissues, within lymph node-like tertiary lymphoid tissue (TLT) [37]. During the first two years of my project, I have investigated the occurrence of TLT in human pancreatic adenocarcinoma (PDAC), one of the most aggressive human malignancies with a dismal survival rate at 5 years [126]. Clinically, PDAC is characterized by low responsiveness to conventional chemotherapy treatments. This feature has fostered the identification of biomarkers to better stratify tumour patients and choose the optimal therapeutic treatment accordingly. Among others, immune mediators have shown to be critical indicators of patients' prognosis in multiple tumour types, including PDAC. Despite the advent of innovative prognostic tools, histo-pathological examination of immune cells in tumours still stands as one of the most powerful approaches to assess their relevance in patients' prognosis. This approach has allowed us to appreciate important features of immune cells related to their distribution in the tumour tissue.

Spatial compartmentalization of T and B lymphocytes within TLT is crucial for recruitment of tumour infiltrating T lymphocytes (TILs) [127], T cell activation and germinal centre reactions, and has been shown to coordinate with TILs infiltration in predicting better clinical outcome [127]. After a preliminary characterization of TLT, we have moved to a more specific analysis of B cells within tertiary lymphoid structures.

B cells play a dual role in cancer progression: while they critically regulate T- cell activation [28], a function highly favoured by the presence of an immune site like TLT, they also release immunosuppressive molecules with the ability to foster cancer development [128]. During the analysis of TLT in human sections, we noticed that B cells localized in two distinct compartments, either scattered in the tumour tissue (B-TILs) or strategically located in association with T cells, within organized lymphoid tissue (B-TLT). Considering the different microenvironment the two B-cell components are exposed to, we hypothesized that they

could exert distinct functions, thus we focused on the duality of this cell population.

These were the main objectives:

- To evaluate the infiltration of B cells in human PDAC specimens.
- To investigate the clinical relevance of B cells in human PDAC according to their spatial distribution in the microenvironment.
- To define the immune features of the tumour microenvironment associated to B cells.

3.2 Occurrence and characterization of TLT in human PDAC

By staining PDAC tissue specimens with anti-CD3 and anti-CD20 antibodies, we appreciated the presence of organized lymphocyte aggregates, mainly localized in the tumour stroma. As previously said, TLT resembles secondary lymphoid organs, since they share the main cellular and molecular components (**Figure 3.1**).

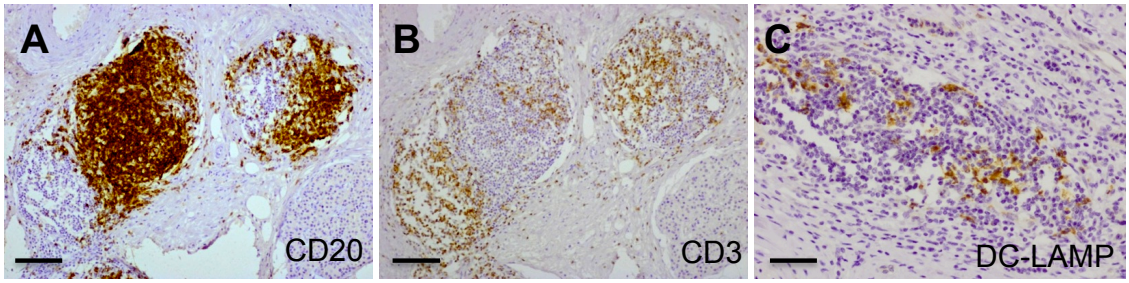

Figure 3.1. Characterization of TLT in human PDAC. In human PDAC tissue specimens, we identified organized lymphoid tissue in the stromal region, composed of compartmentalized B and T cell areas (**A** and **B**) and mature dendritic cells (**C**). Scale bars: 500μm (**A** and **B**); 200μm (**C**).

These structures are not present in the normal pancreatic tissue, thus suggesting that their neo-genesis is related to tumour occurrence. A more detailed characterization of B cell aggregates revealed the presence of distinct B cell (**Figure 3.1, panel A**) and T cell compartmentalized areas (**Figure 3.1, panel B**), containing mature dendritic cells expressing DC-LAMP (**Figure 3.1, panel C**) and PNAd+ high endothelial venules (HEV) (**Figure 3.2, panel A**), thus confirming that they have features of tertiary lymphoid tissue (TLT).

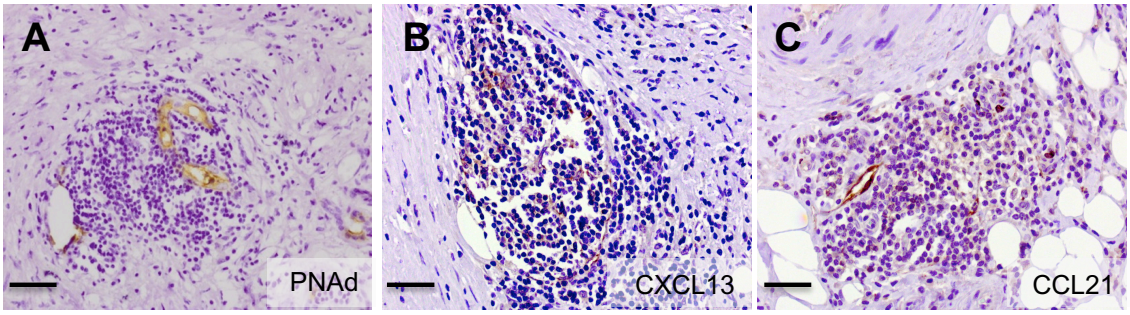

Figure 3.2. TLT in human PDAC is equipped to mediate recruitment of naïve lymphocytes. We confirmed the presence of high endothelial venules (HEV), expressing PNAd (**A**), essential for naïve T-cell recruitment and the presence of the two chemokines CXCL13 and CCL21 fundamental for the maintenance of TLT compartmentalization through recruitment of B and T cells (**B** and **C**). Scale bars: 200μm.

The presence within lymphoid tissue, of the lymphorganogenic chemokines CXCL13 (**Figure 3.2, panel B**) and CCL21 (**Figure 3.2, panel C**), involved in recruitment of B and T cells, suggests an important immunological role for TLT in the recruitment of tumour infiltrating lymphocytes in human PDAC, also confirmed by the presence of Lyve-1 positive lymphatic vessels (**Figure 3.3, panel A**). B cell area was often found to contain a germinal centre expressing both the proliferation markers Ki67 (**Figure 3.3, panel B**) and Bcl-6 (**Figure 3.3, panel C**), suggesting that this immune site is fully equipped to sustain B cell activation in human PDAC.

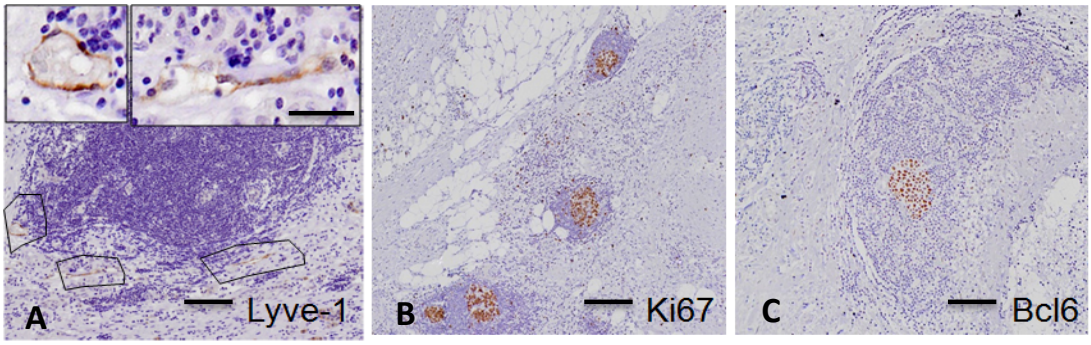

Figure 3.3 Functionality of TLT in human PDAC. We documented the presence of Lyve-1+ lymphatic vessels (**A**), suggesting the possibility of draining tumour antigens; Ki67+ proliferating cells (**B**), an important feature that could indicate the presence of a germinal centre; and Bcl-6, expressed by activated B cells (**C**). Scale bars: 500μm **A**-**C**; 50μm insert in **A**.

3.3 Distinct spatial distribution of B cells in human PDAC

By analysing the occurrence of TLT in human PDAC specimens, we observed that B cells and T cells localize both within and outside such structures. We decided to focus on B cells, because their dual localization could represent an important feature related to their function. Compared to normal pancreas (**Figure 3.4, A**), immunohistochemical analysis of human PDAC specimens with an anti-CD20 antibody revealed a considerable infiltration of $CD20^+$ B lymphocytes (**Figure 3.4, B-D**). As already mentioned, $CD20^+$ cells were found both as irregularly interspersed cells at the tumour-stroma interface (CD20-TILs) (arrowheads in **Figure 3.4, B** and **C**), but also as dense aggregates, displaying a distinct spatial organization, located within the tumour stroma (asterisks in **Figure 3.4**, **panel B and D**). In order to describe the spatial distribution of B cells in PDAC we compared the IRA% of CD20+ cells (**Figure 3.4, E**), focusing on B cell aggregates (CD20-TLT) or infiltrating the tumour-stroma interface (CD20-TILs). This analysis shows that in human PDAC, B cells are preferentially organized in TLT rather than randomly distributed in the tumour tissue.

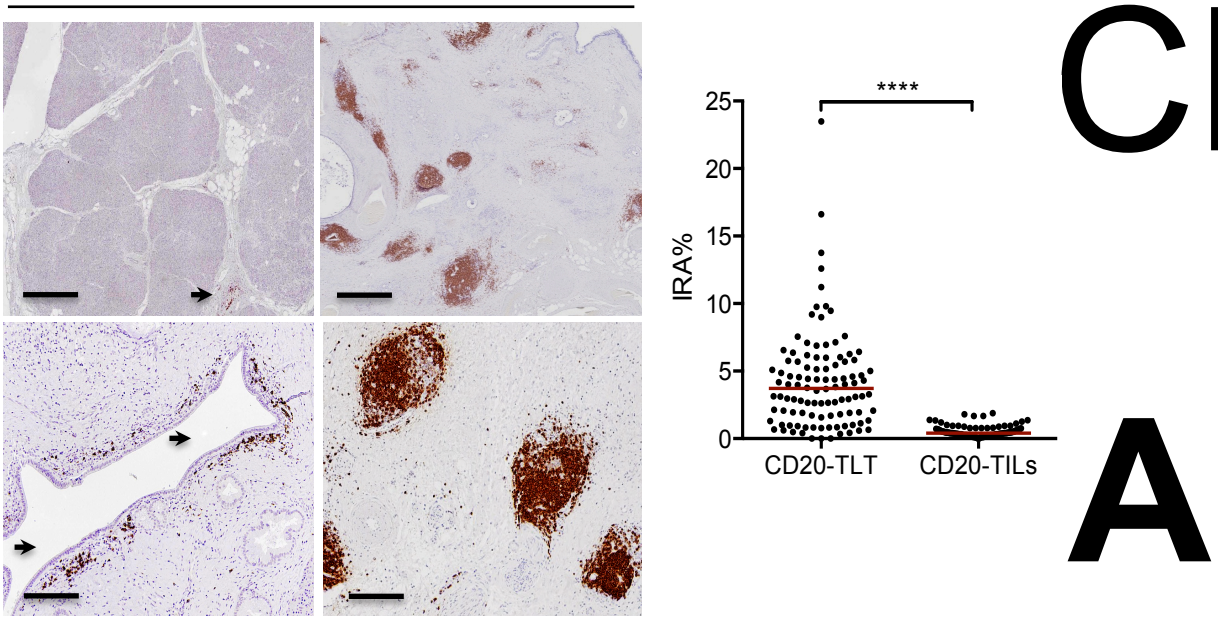

Figure 3.4. B cells strategically localize in tertiary lymphoid tissue in human pancreatic adenocarcinoma. Representative images obtained from virtual digital slides of human normal pancreas (**A**) and pancreatic cancer (**B** and **D**), stained for CD20+ B cells. Staining with an anti-CD20 antibody shows a few B cells scattered in a normal pancreas (arrowhead in **A**) and at the tumour stroma-interface in PDAC (arrowheads in **C**), while the majority of B cells is located within dense aggregates (asterisks in **B** and **D**). Quantitative evaluation of the density of B cells according to their localization within CD20-TLT or as CD20-TILs in tissue specimens from 104 PDAC patients (**E**). Scale bars: 1mm (**A** and **B**)**; 500**μm (**C** and **D**). Red lines represent mean; p-value calculated by Student's *t* test ****: p<0,0001 (**E**).

3.4 Dichotomy of B cell prognostic impact in human PDAC

I next asked whether the dual pattern of B-cell infiltration within pancreatic tissue reflects a distinct prognostic value. Therefore, the clinical significance of B cells in human PDAC was assessed considering CD20-TLT and CD20-TILs as two distinct populations. In a retrospective study, I have quantitatively evaluated the percentage of immune-reactive area (IRA%) of the CD20-TLT and CD20-TILs at the tumour-stroma interface, in 104 tissue specimens from consecutive, non-metastatic PDAC patients (**Table 2**). CD20-TLT immuno-reactive area (IRA%) ranged from <0.05% to 23.49%, with a median value of 3.72% (second–third quartiles, 1.71%-5.71%), while CD20-TIL IRA% ranged from <0.05% to 1.89%, median value 0.41% (second-third quartile 0.26%-0.69%) (**Table 2**). We recorded 38 events of disease specific death (DSS) in 104 PDAC patients, during the follow-up period of the study. Cox multivariate analysis showed that nodal status and grade associated to prognosis; notably, among the immune variables analyzed, B cells were independently associated to prognosis, but their prognostic value diverged according to their spatial distribution in the tissue. CD20-TLT associated with better prognosis (OR=0.24; 95% CI (0.08-0.71); P=0.010, 4th versus 1st quartile; **Table 5**), while CD20-TILs associated to worse prognosis (OR=2.56; 95% CI (0.91-7.23); P=0.07, 3rd versus 1st quartile; **Table 5**). This result highlights B cells as prognostic variables in human PDAC and suggests that the

influence of B cells on tumor progression changes whether they are confined within lymphoid tissue or are scattered at the tumour-stroma interface. Kaplan-Meier survival analysis showed that only high density of CD20-TLT (2^{nd}-4^{th} quartiles versus 1^{st}) correlated with a better prognosis (median survival 16.9 mo CD20-TLT^{hi} versus 10.7 mo CD20-TLT^{lo}; P=0.0085; n=104; **Figure 3.5, panel A**), while high CD20-TIL density (3^{rd}-4^{th} versus 1^{st}-2^{nd}) had a propensity to associate to worse prognosis but not significantly (median survival 12.7 mo CD20-TILs^{hi} versus 18.9 mo CD20-TILs^{lo}; P=0.115; n=104; **Figure 3.5, panel B**). When the two variables were considered concomitantly, the immune signature comprising CD20-TLT^{hi} /CD20-TIL^{lo} robustly predicted longer survival (median survival 30.9 mo CD20-TLT^{hi}/CD20TILs^{lo} versus 14.1 mo any other; P=0.0051; n=104; **Figure 3.5, panel C**). This confirmed that the spatial distribution of B cells dictates their prognostic behaviour, and suggested that only B cells sequestered within a lymphoid tissue contrast tumour progression.

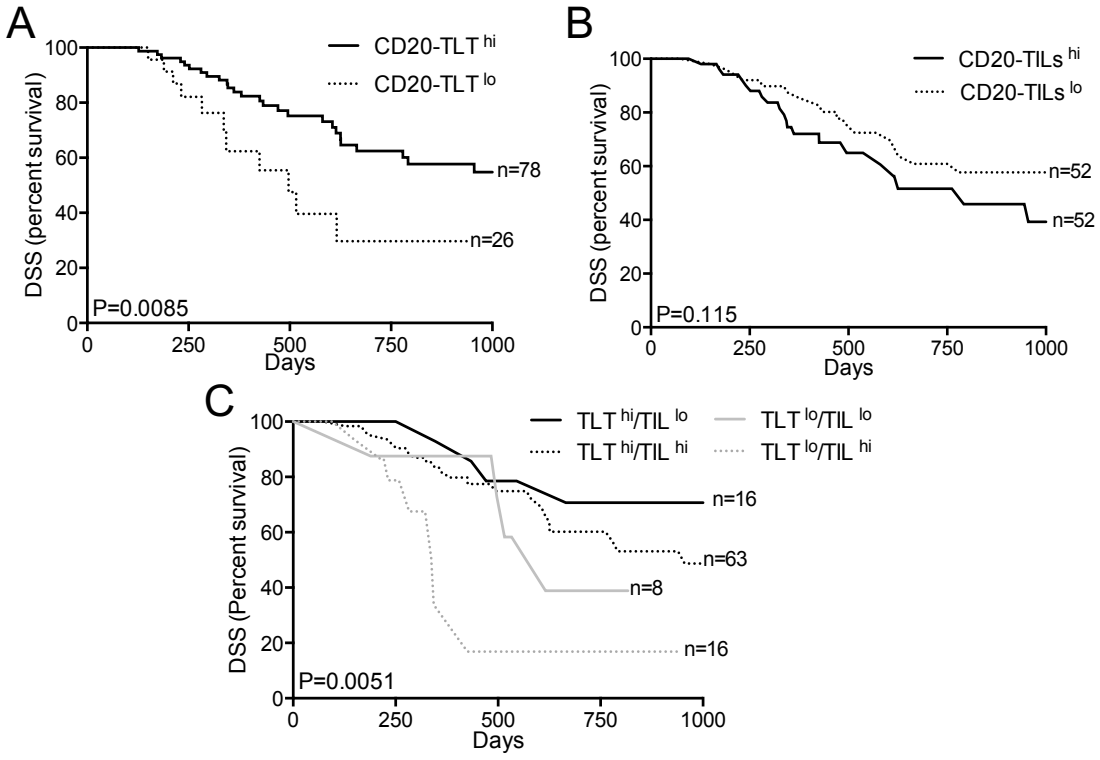

Figure 3.5. B cell spatial organization impacts on human PDAC prognosis. Distinct spatial localization of B cells in the tumour microenvironment dictates their prognostic behaviour. Kaplan-Meier survival analysis shows correlation of longer disease specific survival (DSS) with high density of CD20-TLT (2nd-4th quartiles) (P=0.0085; n=104) (**A**),

while high density of CD20-TILs (3rd-4th quartiles) shows a tendency to associate to worse prognosis (P=0.115; n=104) (**B**). The immune signature comprising CD20-TLT^{hi}/CD20-TILs^{lo} robustly predicts longer survival (P=0.0051; n=104) (**C**). P-value by Wilcoxon-Mantle Cox test.

		Univariate Analysis [a]		Multivariate Analysis [a]	
		H.R. (95%C.I.)	P	H.R. (95%C.I.)	P
Patient Demographics					
Age	< 50 yrs	1.00 ref.			
	50-70 yrs	2.13 (0.49-9.29)	0.312		
	≥ 70 yrs	4.22 (0.98-18.13)	0.053		
Gender	Female	1.00 ref.			
	Male	1.09 (0.58-2.07)	0.782		
Tumor Features					
Nodal involvement	No	1.00 ref.		1.00 ref.	
	Yes	2.13(1.03-4.41)	**0.020**	2.63 (1.17-5.90)	**0.01**
	na				
Grade [c]	G1/G2	1.00 ref.		1.00 ref.	
	G3/G4	2.74 (1.37-5.49)	**0.004**	2.50 (1.20-5.24)	**0.015**
	na				
Radical surgery	No	1.96 (0.93-4.14)	0.078		
	Yes	1.00 ref			
	na				
Chemotherapy (CTX)					
Adjuvant treatment	No	1.00 ref			
	Yes	1.03 (0.52-2.04)	0.942		
Tumor Immune features					
CD20-TLT (quartiles)[b]	1st (0-1.71)	1.00 ref.		1.00 ref.	
	2nd (1.71-3.72)	0.40 (0.16-0.98)	**0.045**	0.41 (0.15-1.09)	0.075
	3rd (3.72-5.71)	0.38 (0.16-0.94)	**0.035**	0.25 (0.09-0.72)	**0.011**
	4th (5.71-	0.40 (0.16-0.98)	**0.044**	0.26 (0.09-0.72)	**0.010**
CD20-TILs (quartiles)[b]	1st (0-0.26)	1.00 ref.		1.00 ref.	
	2nd (0.26-0.41)	1.30 (0.50-3.36)	0.594	1.49 (0.53-4.19)	0.449
	3rd (0.41-0.69)	2.88 (1.18-7.03)	**0.020**	2.85 (1.05-7.78)	**0.040**
	4th (0.69-1.89)	1.23 (0.46-3.30)	0.674	1.88 (0.58-6.03)	0.289
CD8-TILs (quartiles) [b]	1st (0.0-0.34)	1.00 ref.			
	2nd (0.34-0.61)	0.51 (0.22-1.23)	0.135		
	3rd (0.61-1.15)	0.89 (0.39-2.07)	0.797		
	4th (1.15-3.42)	0.69 (0.27-1.77)	0.445		
PD-1 GC	Yes	1.00 ref.			
	No	1.47 (0.72-2.99)	0.285		

[a] COX regression analysis
[b] Densities as percent immunoreactive area at the tumor-stroma interface
[c] G1/G2, well-to moderately differentiated; G3, G4 poorly differentiated

Table 5. Predictors of post-surgical disease specific survival in cohort 1 patients with pancreatic ductal adenocarcinoma

3.5 Confinement of B cells within TLT associates to a germinal centre immune signature

To understand whether the immune signature could be affected by the localization of B cells, I analysed the expression of immune related genes in the whole tissue section. Since analysed specimens were of similar size, and were previously selected in the same tumour region (within resected tumour lesion), PDAC patients were selected exclusively using B cell infiltration. RNA was extracted from tumors displaying very high density of TLT (4^{th} quartile; TLT^{hi}) and compared to tumours with very high density of TILs (4^{th} quartile; $TILs^{hi}$). Non-tumour pancreatic tissue was taken as control tissue (Normal). PDAC specimens with high density of TLT showed major changes in genes related to germinal centre reaction (activation-induced cytidine deaminase (*AICDA*), B cell recent activation (*CD27*), B-cell signalling (B-cell linker (*BLNK*)), B-cell differentiation and proliferation (interleukin-7 (*IL7*) and interleukin-2 (*IL2*)) and B-cell responses (interleukin-13 (*IL13)*) (**Figure 3.6**). Notably, while TLT^{hi} PDAC samples exhibited a significant increase in genes related to T-cell infiltration (*CD8B*) and activation (*IL-12*), suggesting that the presence of B cells within TLT was also regulating T cell recruitment and activation, $TILs^{hi}$ samples exhibited increased expression in immunosuppressive genes, including programmed cell death-1 ligand (PDL-1 or *CD274), CCR4* and transforming-growth factor-beta (*TGF-β).*

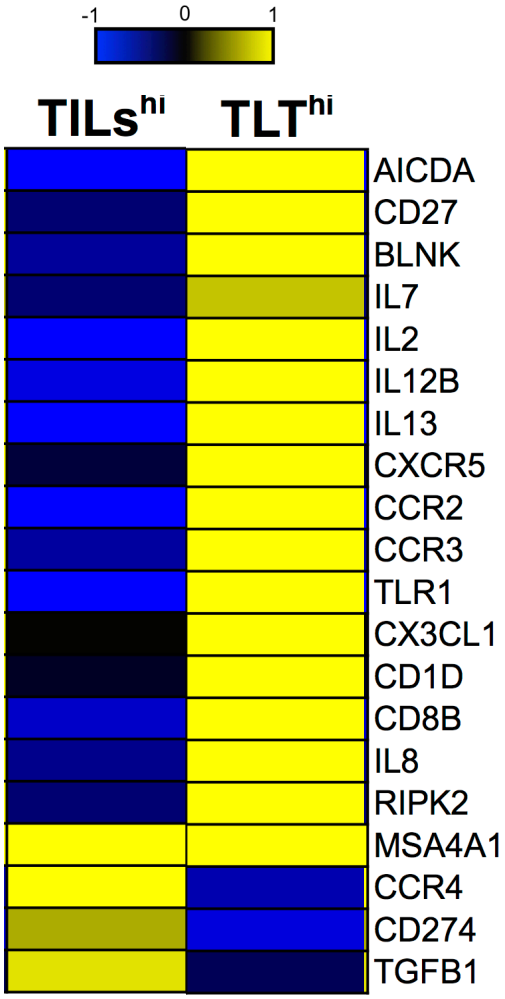

Figure 3.6 Heatmap showing the immune signature of human PDAC specimens with different CD20-TLT density. RNA was extracted from paraffin embedded tissue specimens of human PDAC, categorized as TLT^{hi} (n=3) or $TILs^{hi}$ (n=3) after immunohistochemical evaluation with an anti-CD20 antibody. RNA from normal pancreata (n=3) was obtained as a control. Sample grouping followed the pattern of B cell distribution (i.e. TLT^{hi} versus $TILs^{hi}$ samples segregating together), suggesting that B cell infiltration identifies specific gene expression programs. A z-score has been calculated for each gene. The color bar refers to increased scores (yellow) and decreased (blue), with intensity encoding magnitude.

Immunohistochemical analysis confirmed that B cells within TLT were often engaged in a germinal centre reaction, as evidenced by Ki67 immunostaining (arrowheads in **Figure 3.7**, **A**) and B-cell lymphoma 6 protein (Bcl-6) (arrowhead in **Figure 3.7**, **B**).

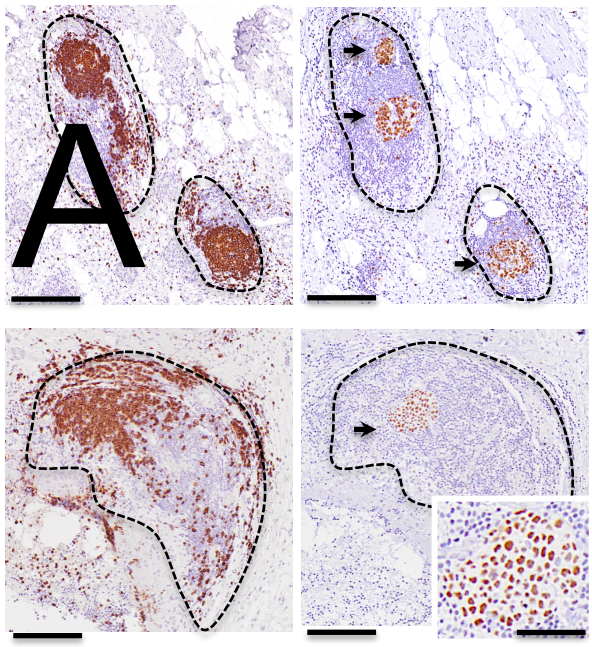

Figure 3.7 Presence of germinal center in CD20-TLT. B cells within TLT are engaged in a germinal center reaction, as evidenced by Ki-67 (arrowheads in upper right panel) and Bcl6 (arrowhead in lower right panel) staining within CD20-TLT (left panels). Sections represented in **A** or **B** are consecutive sections. Scale bars: 500μm and 200μm (insert in panel **B**).

B

CD20

3.6 Confinement of B cells within TLT correlates with CD8-TIL infiltration, and empowers their favourable prognostic value

$CD8^+$ T cells are an essential constituent of the antitumor immune response. In light of the association between TLT and CD8 in gene expression analysis, I assessed the density of tumour-infiltrating $CD8^+$ T-cells (CD8-TILs) in cohort 1 PDAC patients. Notably, whole tissue visualization of $CD8^+$ infiltrating cells evidenced a higher density of CD8-TILs in tissues with a high density of TLT (arrowheads in **Figure 3.8, A**). In fact, density of CD20-TLT correlated with the IRA% of CD8-TILs (r=0.29, P=0.009, n=104) (**Figure 3.8, B**), consistent with the ability of TLT to mediate recruitment of lymphocytes.

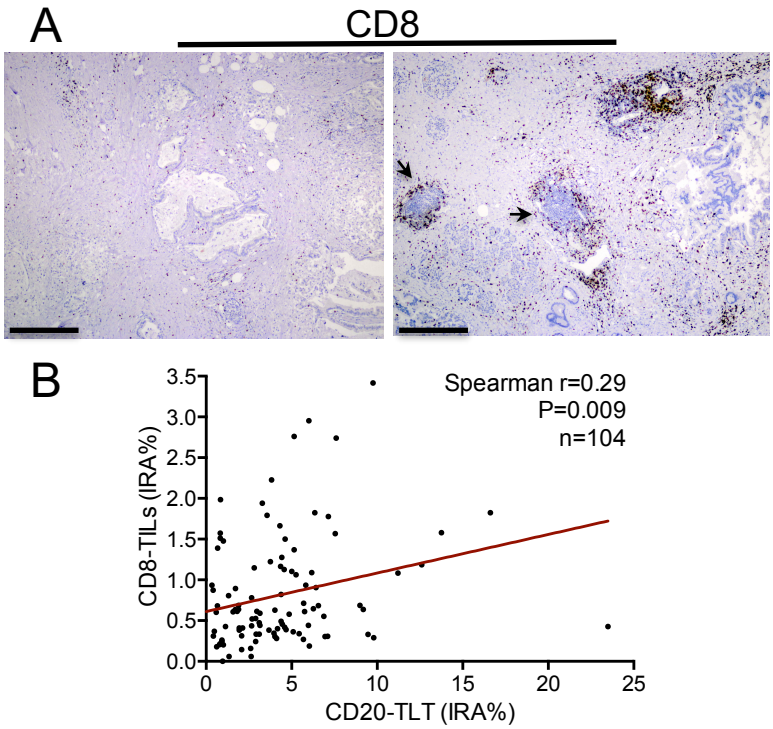

Figure 3.8. Confinement of B cells within TLT correlates with CD8-TIL infiltration. (**A-B**) CD20-TLT correlates with density of $CD8^+$ T cells in human PDAC. Representative images of human PDAC specimens stained with an anti-CD8 antibody show a high density of $CD8^+$ cells in tissues with TLT (**A**). Density of CD20-TLT (IRA%) linearly correlates with density of CD8-TILs (IRA%) (r=0.29, P=0.009, n=104) (**B**). Scale bars: 500μm.

While CD8-TILs were not associated to prognosis on their own (median survival 15.5 mo CD8-TILs^{hi} versus 14.2 mo CD8-TILs^{lo}; P=0.254, n=104) (**Figure 3.9, A** and **Table 5**), a concomitant high density of both CD8-TILs (2nd-4th quartiles) and CD20-TLT (2nd-4th quartiles) identified a subgroup of patients with better outcome compared to all other patient groups (median survival 17.9 mo CD20-TLT^{hi}/CD8-TILs^{hi} versus 12.2 mo CD20-TLT^{lo}/CD8-TILs^{hi}; P=0.031, n=104) (**Figure 3.9, B**), suggesting that the presence of tertiary lymphoid tissue empowers the prognostic function of CD8^{+} T cells.

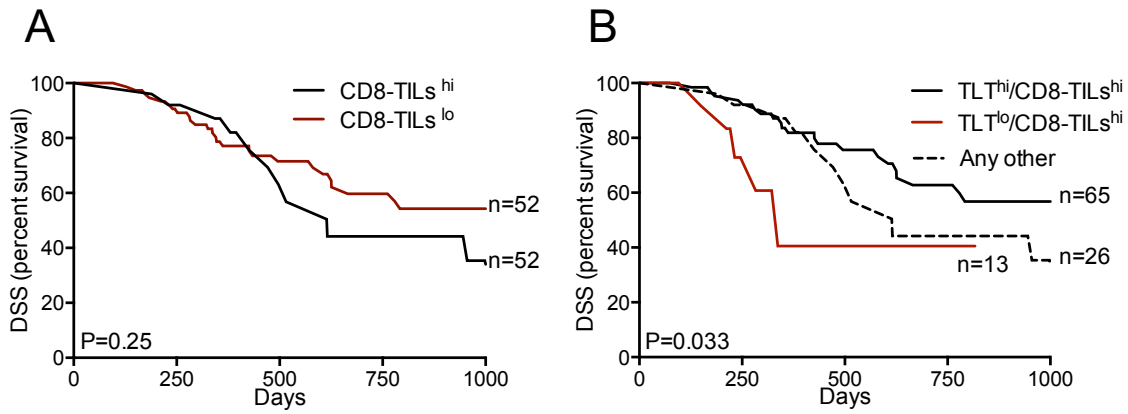

Figure 3.9. Confinement of B cells within TLT empowers the favourable prognostic value of CD8-TILs. Kaplan-Meier curves showing that while high density of CD8-TILs (2nd-4th quartiles) is not significantly associated to prognosis (P=0.254, n=104) (**A**) concomitant high density of CD8-TILs (2nd-4th quartiles) and high density of CD20-TLT (2nd-4th quartiles) identifies a subgroup of patients with longer disease-specific survival (P=0.031; n=104) (**B**). Bars: 500 μm (**A**).

3.7 Characterization of intratumour TLT after antigen-specific immunotherapeutic vaccination in a preclinical model of PDAC

The presence of immunologically active TLT could be of remarkable importance in the perspective of inducing a local antitumor immune response. I have therefore investigated whether an immunotherapeutic approach could induce formation of TLT in a genetic preclinical model of PDAC. This model is very suitable to recapitulate the microenvironment of PDAC, compared to subcutaneous models, although tumour development is slower. We took advantage of the collaboration with the group of Professor F. Novelli, at the University of Turin, who is studying the effect of a DNA-based vaccination protocol on tumour infiltrating leukocytes. The DNA-based vaccine is composed of a plasmid coding for α–enolase (ENO1), an enzyme strongly expressed by PDAC cells with high immunogenicity potential [124]. The plasmid is then electroporated into the femoral muscle of KC mice (i.e. mice bearing the tumorigenic $Kras^{G12D}$ mutation, only in pancreatic cells), in order to force the expression of ENO1 in a peripheral organ. Vaccination of tumour-bearing mice has been shown to have a protective effect in this preclinical model [124]. In particular, anti-ENO1 vaccination promoted the antigen-specific immune response increasing. So far I have been able to analyse only a few mice and I have observed that TLT neo-genesis is significantly induced in vaccinated mice (pENO) compared to both control groups (empty vaccine (pEmpty) treatment and unvaccinated mice (Ctrl)) (**Figure 3.10**). This suggests that the antigen stimulation, mediated by the vaccination protocol, drives TLT formation by promoting both recruitment and spatial organization of lymphocytes in the microenvironment.

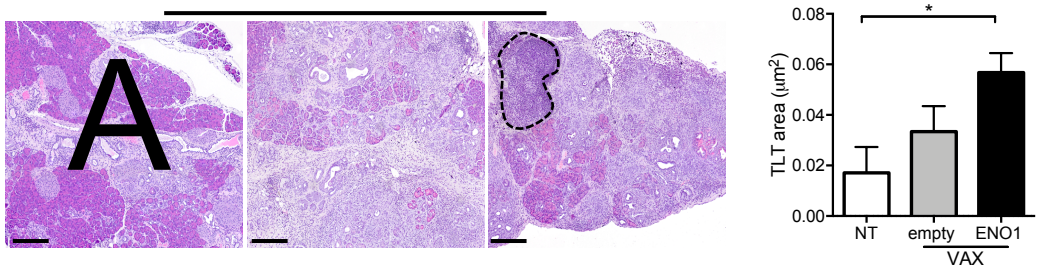

Figure 3.10. An immunotherapeutic DNA-vaccine induces neo-genesis of intratumour TLT in a preclinical model of PDAC. Induction of TLT by an antitumor vaccination in Kras^{G12D}-Pdx1-Cre mice. Histological sections of murine PDAC from non-treated mice (NT; n=10) or mice vaccinated with empty vector (empty; n=4) or a vector encoding ENO1 (ENO1; n=7) stained with hematoxylin-eosin (dotted line indicates an intratumour TLT) (**A**). Graph refers to the area occupied by TLT (**B**). P-value by Students' t test; Horizontal Bars represent mean, vertical bars SEM; *: P<0.05; Scale bars: 500μm.

The increase was paralleled by an increase in CD3-TILs, suggesting that induction of TLT by immunotherapeutic approaches could be strategic to increase recruitment of T cells (**Figure 3.11**).

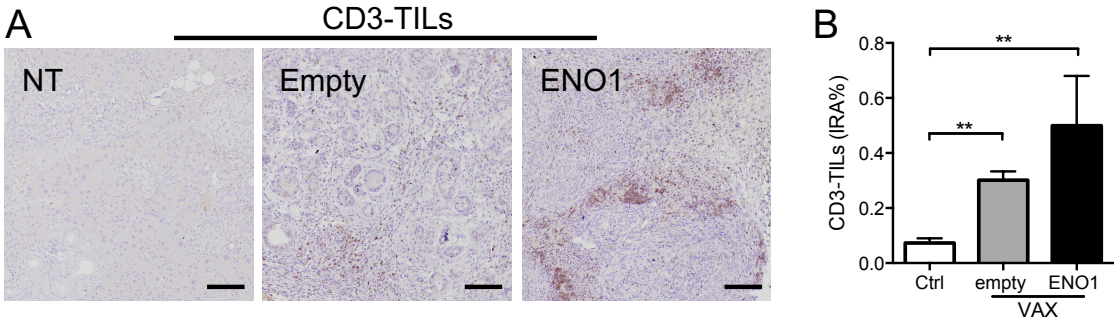

Figure 3.11. An immunotherapeutic DNA-vaccine induces increased recruitment of T cells in a preclinical model of PDAC. Histological sections of murine PDAC from non-treated mice (NT; n=10) or mice vaccinated with empty vector (empty; n=4) or a vector encoding ENO1 (ENO1; n=7) stained with anti-CD3. IRA% of CD3-TILs (**A**) is significantly increased by vaccination compared to untreated mice (**B**). P-value by Students' t test; bars represent SEM; **: P<0.001. Scale bars: 100μm.

Importantly, vaccination generated a pool of long-lived T cells specific for ENO-1 and able to secrete IFN-γ after *in vitro* exposure to cognate antigen, only in ENO1-vaccinated mice compared to mice vaccinated with the empty vector (**Figure 3.12**).

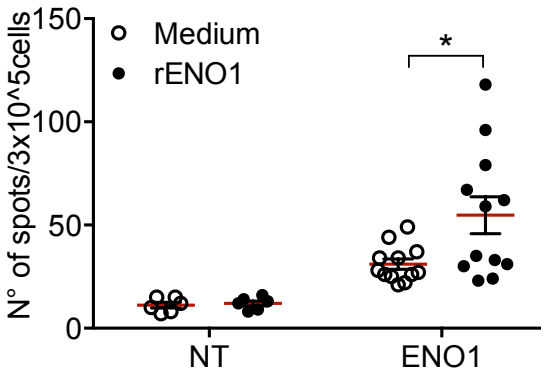

Figure 3.12. ENO1 vaccination induces specific T cell response. Spleen cells from untreated or ENO1-vaccinated mice were stimulated on an enzyme-linked immunosorbent spot plate in the presence (black dots) or absence (white dots) of rENO1. Anti-ENO1 T cells are significantly induced in ENO1-vaccinated mice (ENO1 n=2), but not in untreated mice (NT; n=2). Numbers in the graph represent the mean number of specific spots (rENO1) normalized to the background (Medium). All conditions were performed in triplicate. Red lines represent mean, vertical bar SEM; $P<0.05$ (*) by Students' t test; all conditions were in quadruplicate.

3.8 Targeting tumour infiltrating B cells unleashes the antitumour immune response in murine PDAC

To further investigate the contribution of scattered tumour infiltrating B cells (B-TILs) on PDAC, we needed to discriminate between B cells that are interspersed versus those that are organized in tertiary lymphoid tissue, either finding a strategy selectively targeting one of those, or alternatively, adopting a model in which only one of the two B populations is present. We reached the conclusion that targeting B cells with an anti-CD20 antibody in an orthotopic model could well fulfil our requirements. The anti CD20 antibody, in fact, has been shown to selectively target B-TILs and spare B cells within lymphoid tissues [111, 112]. I tested the effect of an anti-CD20 antibody targeting B cells (clone 5D2, Genentech) in an orthotopic implantable model of PDAC, treating the mice with the antibody 3 days post tumour injection. Differently from the genetic model previously mentioned, I did not observe formation of B-TLT in any of the tumour-bearing mice, likely due to the rapid tumour growth (21 days) and to the absence of a chronic inflammatory reaction. In contrast, scattered B cells still infiltrated the tumour tissue, confirming that B-TILs act independently from B-TLT

in this preclinical model. Circulating B cells were dramatically depleted by a single injection of the antibody (**Figure 3.13, A**), and the effect persisted until the end of the experiment (**Figure 3.13, B**), while the number of other circulating leukocytes (including $CD3^+$ T cells and $CD11b^+$ myeloid cells) was not significantly affected (**Figure 3.14, A-B**).

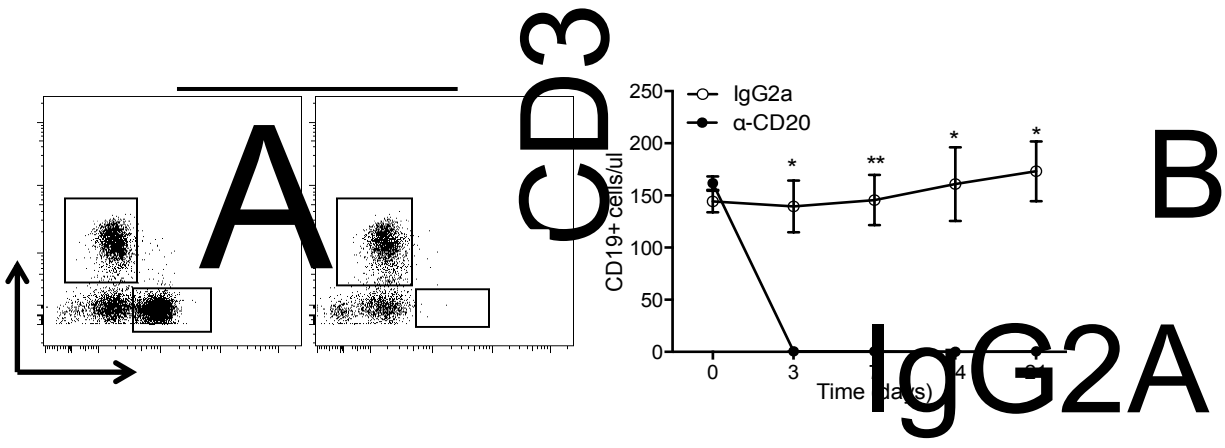

Figure 3.13. Depletion of B cells by an anti-CD20 antibody in a murine implantable PDAC model. Mice were orthotopically injected with the PDAC cell line Panc02 and administered either an irrelevant antibody (IgG2A) or α-CD20 on day 3 post injection. (**A**) Exemplificative FACS plot showing depletion of circulating blood $CD19^+$ B cells. (**B**) B cell depletion started at day 3 and lasted until the end of the experiment. Means relative to one of three independent experiments is shown (n=3 mice, IgG2A; n=4 mice α-CD20); bars represent SEM; P<0.05 (*), P<0.001 (**) and P=ns refer to Students' t test.

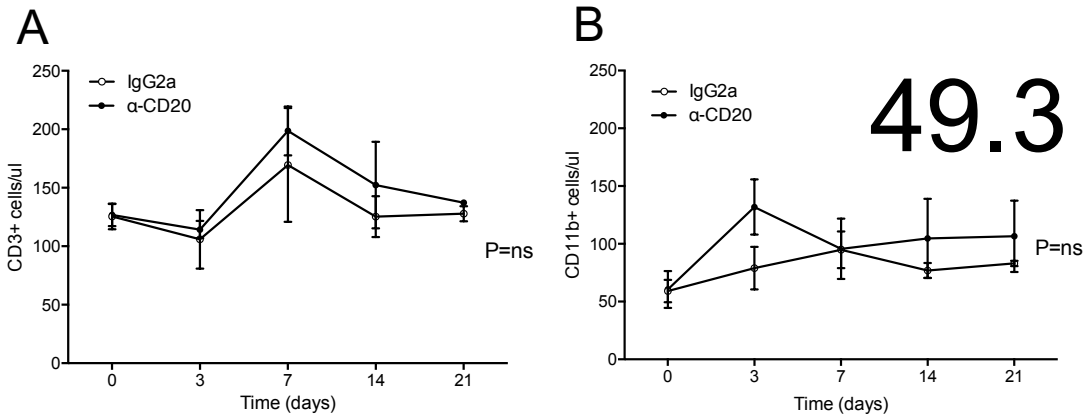

Figure 3.14. **Blood cell counts after α -CD20 treatment.** Mean counts of circulating $CD3^+$ T cells (**A**) and $CD11b^+$ myeloid cells (**B**) in IgG2A (n=3) and α-CD20 treated (n=3) mice, at different time points. Bars represent SEM; P<0.05 (*), P<0.001 (**) and P=ns refer to Students' t test.

Consistent with the reduction of circulating B cells, also the number of B-TILs scattered in the tumour microenvironment was significantly reduced by the treatment (**Figure 3.15, left panel**). This confirmed that the depletion of circulating B cells is sufficient to prevent the accumulation of these cells in the tumour microenvironment, providing a valuable tool to dissect the role of B-TILs in this preclinical model of PDAC. The tumour volume was measured in α-CD20 treated and control tumour bearing mice (**Figure 3.15, right panel**). Despite a profound depletion of B-TILs, α-CD20 treatment alone was not sufficient to significantly reduce the tumour growth. This might suggest that B-TILs are only indirectly involved in controlling tumour growth, for instance by sustaining functions of other effector immune cells.

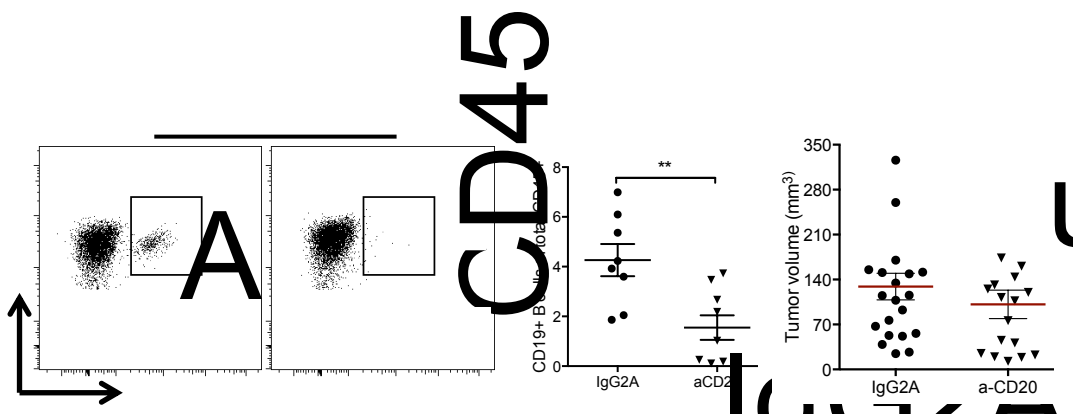

Figure 3.15. Targeting tumour infiltrating B cells unleashes immune response in murine PDAC. (**A**) Exemplificative FACS plot showing depletion of tumour infiltrating $CD19^+$ B cells. (**B**) Percentage of $CD19^+$ B cells infiltrating PDAC tumours is reduced by α-CD20 treatment. One of three experiments performed is shown (n=8 mice, IgG2A; n=9 mice α-CD20; bars represent SEM; P=0.004 by Students' t test). (**C**) Tumour growth was slightly but not significantly reduced by α-CD20 treatment. Mean of three independent experiments is shown: n=20 mice, IgG2A; n=16 mice α-CD20; bars represent SEM; P<0.05 (*), P<0.001 (**) and P=ns refer to Students' t test.

I decided to dissect the contribution of B-TILs to the anti-tumour immune response in this orthotopic model of PDAC by comparing the immune signature of the leukocyte population isolated from PDAC tumours from control and B-TILs depleted (α-CD20-treated) mice. Depletion of B-TILs resulted in a significant increase in genes related to T cell and NK cell infiltration (*CD4*, *CD8*, *NCR1*), activation (*GMZA*, *GMZB*, *IL12, IFNG,* and *TNFA*) and

recruitment (*CXCR3*) (**Figure 3.16**). These results show that, in an implanted tumour model devoid of TLT, depletion of B-TILs increases the recruitment of important components of the antitumor immune response.

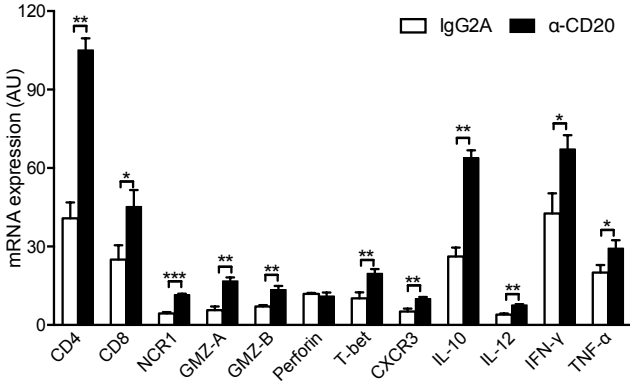

Figure 3.16. Immune signature after α-CD20 treatment. RNA from leukocytes isolated from PDAC of mice treated with IgG2A or α-CD20 shows induction of genes related to T cell infiltration and activation. Mean of three independent experiments is shown: n=4 mice, IgG2A; n=4 mice α-CD20; bars represent SEM; P<0.05 (*), P<0.001 (**) refer to Students' t test.

To gain more insight on the biological relevance of the signature obtained, the set of genes was interrogated by a systems biology approach based on Ingenuity Pathway Analysis (IPA, http://www.ingenuity.com). Surprisingly, within the panel of genes analysed, depletion of B cells with α-CD20 induced a significant functional enrichment of genes involved in lymphoid tissue structure and development, $CD8^+$ T cell infiltration and maintenance and differentiation of T cells (**Figure 3.17**). Together, those findings confirmed that upon B-TILs depletion mRNA levels of key T cell effector genes are significantly increased, suggesting that in this model B-TILs might impair effector functions of T cells.

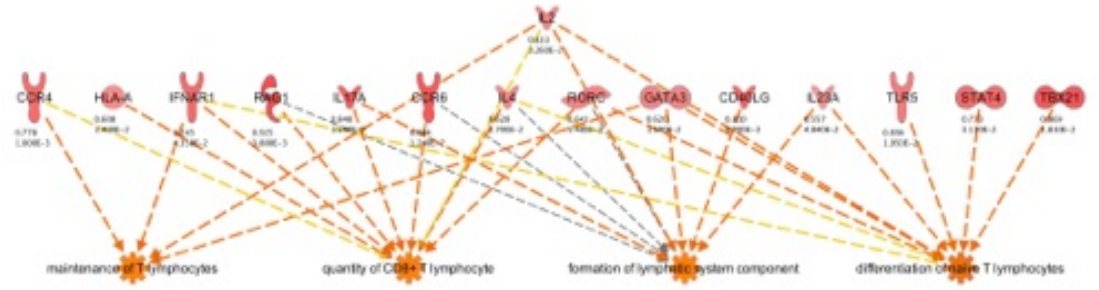

Figure 3.17. Immune signature after α-CD20 treatment. Systems biology analysis showing the relationship between molecules and biological functions based on the genes modulated after depletion of B cells. The analysis highlights significant activation of biological functions related to lymphoid tissue structure and development, CD8+ T cell infiltration and maintenance and differentiation of T cells.

3.9 Discussion

In this first section, I have addressed the occurrence of TLT in the tumour microenvironment of pancreatic cancer, its ability to promote anti-tumour immune responses and its relevance as a prognostic immune variable and in the design of novel immunotherapeutic strategies. Important point of novelty of this work relates to the distinct assessment of an immune population (B cells in this case) in the tumour microenvironment, according to its spatial distribution. We show that the prognostic behavior of B cells in PDAC is tightly linked to their topological organization within the microenvironment. This dual spatial organization may reflect a distinct function. The strategic localization of B cells in association with T cells within highly organized lymphoid tissue could reflect how B and T cells interact during the organization of a local immune response. B cells can modulate the immune response by mechanisms involving cytokine secretion and antigen presentation [28, 129]. Also, B cells within a lymphoid site associated to a follicular signature, suggesting that they could be involved in an ongoing follicular immune response with a protective antitumor role. Finally, CD20-TLT correlated with $CD8^+$ T cell infiltration, suggesting that B cells within TLT could concomitantly be engaged in humoral and T cell responses. Overall, several immunotherapeutic approaches are under evaluation in human PDAC, including vaccination protocols directed against PDAC antigens, which would benefit from a microenvironment favourable for TLT induction.

As to the CD20-TIL component, on the basis of our clinical and preclinical data we hypothesize that the egress of B cells into the tissue is detrimental to an effective anti-tumour response and might reflect a non-specific pro-tumour inflammatory reaction. In accordance, the depletion of tumour infiltrating B cells was sufficient to reinstate a genetic signature associated to an effective $CD8^+$ antitumour immune response in a PDAC preclinical model without TLT. The role of B cells in the progression of solid tumours has fostered studies concerning their targeting by anti-CD20 antibodies [130-135]. Based on our data, the design

of anticancer strategies envisaging the depletion of B cells should take into account the possibility to selectively target CD20-TILs but not CD20-TLT.

In addition to our findings, the depletion of B cells has been reported to produce contrasting effects according to tumour setting and depletion strategy. In mice genetically devoid of B cells both the spontaneous and the therapeutic vaccination-induced immune response against tumour were enhanced compared to wild-type mice [135-141]. On the contrary, in transplantable tumour models, the anti-CD20 mediated acute depletion of B cells showed variable effect according to tumour cell line used [142-144]. While the impact of B cell targeting over tumour growth is clearly established, the mechanisms involved in determining a positive or negative role of B cell targeting need further investigation. Interestingly, the kinetic of B cell depletion by anti-CD20 antibodies varies among different B cell sub-populations (i.e. circulating, marginal zone, peritoneal) [131]. Thus, it is reasonable to suppose that contradictory effects of B cell depletion observed in preclinical models of tumor might reflect differential contribution of B cells subsets in coordinating the immune response. Moreover, in non–tumor conditions, anti-CD20 therapy has resulted ineffective in depleting $CD20^+$ cells in tertiary lymphoid organs [130], suggesting that B cells might receive survival signals within lymphoid niches [131]. The differential sensitivity that B cells display to anti-CD20 treatment according to their differentiation status and localization could be exploited to design tailored approaches, assuming that a rigorous evaluation of B cell spatial distribution is performed.

4. Effect of tumour metabolism on immune infiltrate

4.1 Background and goal

Among the most important interactions occurring in the tumour microenvironment, the pathways that regulate immune cell function and metabolism are tightly linked [94, 145, 146]. Energy and biosynthetic precursors are essential for T cell immune function in homeostatic conditions [147]; as a result, metabolic dysfunction, which is often associated to pathologic states, impacts on the efficacy of the immune response. The condition of nutrient deprivation is commonly present in tumour settings, suggesting that metabolic microenvironmental cues could potentially impact on the fulfilment of an effective antitumor immune response [1]. Overall, metabolic reprogramming is considered a hallmark of cancer progression [1, 91] and its therapeutic modulation is emerging as a strategy to ameliorate the antitumour immune response [148].

PDAC cells escape immune recognition and devise an immunosuppressive microenvironment, by mechanisms including limited immunogenicity, inadequate immune cell infiltration and myeloid immune-regulatory networks [88, 149, 150]. However, surprisingly, the influence of metabolic cues on immune cell function has not been addressed.

In an effort to characterize environmental factors affecting immune cell function, in this part of the project, I have investigated the relationship between the tumour metabolic profile and the immune response in human PDAC, with the following main objectives:

- Dissecting the influence of tumour metabolism over infiltrating immune cell phenotype in human PDAC
- Inhibit tumour glycolysis to evaluate potential therapeutic implications in preclinical models of PDAC
- Combine Immunotherapy with tumour glycolysis inhibiting strategies

4.2 Metabolomics analysis of pancreatic juice indicates an alteration in glucose metabolism in pancreatic ductal adenocarcinoma patients

Pancreatic juice is the liquid that collects the secretions of pancreatic duct and acinar cells. It contains pancreatic digestive enzymes and a high concentration of bicarbonate ions, essential to neutralize gastric acid, and to allow proper enzymatic activity. Pancreatic juice can be readily sampled from the main pancreatic duct both during pancreasectomy, and with other less invasive procedures (**Figure 4.1, A**) [151]. Cancer cells present metabolic alterations that could result in modification of biological fluids and, in the case of PDAC, such alterations could modify the composition of ductal cell secretions. In order to get a comprehensive overview of the altered metabolic profile of PDAC specimens, we compared the metabolite content of pancreatic juice obtained from patients with pancreatic adenocarcinoma to control patients with pancreatic pathologies histologically distinct from PDAC (including pancreatitis, neuroendocrine tumours, papillary tumours). We collected pancreatic juices from 40 patients who underwent pancreasectomy at our Institute (**Figure 4.1, B**). The patient cohort (Cohort 2. **Table 3**) included 31 PDAC and 9 other non-PDAC pathologies (4 papillary-ampulla tumours, 2 pancreatitis, 2 neuroendocrine tumours, 1 intraductal papillary mucinous neoplasm (IPMN)). We then obtained a broad metabolic picture of PDAC specimens by performing a metabolomics study using 1H nuclear magnetic resonance (NMR) spectroscopy. Due to the unexplored properties of pancreatic juice, we chose NMR, since compared to other metabolomics assays (e.g. liquid chromatography and mass spectrometry, LC-MS) it is less sensitive, though more accurate in identifying metabolites. In particular, we collected both one-dimensional (1d) Nuclear Overhauser Effect Spectroscopy (NOESY) and 1d Carr-Purcell-Meiboom-Gill (CPMG) spectra [152] on 40 pancreatic juice samples. As depicted in **Figure 4.1, C**, we employed the CPMG spectra for multivariate statistical analysis (PDAC in blue, non-PDAC in green), which allow us to

appreciate the details of the smaller molecular weight metabolites by filtering the broad NMR signals of macromolecules (e.g. lipoproteins, lipids etc.). After spectral bucketing (0.02 ppm buckets width) by AMIX software (Bruker Biospin), a total spectral area normalization took place for all buckets in order to avoid any dilution differences between the samples. Subsequently, a supervised OPLS-DA (orthogonal projection latent structure discriminant) analysis segregated the two groups (**Figure 4.1, D**), with an accuracy of more than 80% obtained by cross-validation (**Figure 4.1, E**), indicating that pancreatic adenocarcinoma could be singled out from other pancreatic pathologies through metabolic profiling. The produced latent variables plots (LV) of the OPLS-DA analysis components and the estimated variable importance in the projection (VIP) score of each group (variables with VIP > 1.0 were initially considered significant for each model) were used for the detection of the weighted variables (NMR signals–buckets), responsible for the group classification. These signals corresponded to the metabolites reported in Figure 1D. The statistical significance (p) of each metabolite was calculated by univariate one-way ANOVA analysis, extra refined by an n-fold cross-validation implementation, by splitting the data into n sub-datasets while performing the ANOVA test (e.g. cross-validated ANOVA) [153]. The fold change of the concentration of 18 metabolites (**Figure 4.1, F**), measured by their NMR signals deconvolution-integration, showed that only concentration of lactate, the end product of glycolysis, resulted increased in PDAC patients, suggesting a selective alteration of glucose metabolism in ductal carcinoma cells.

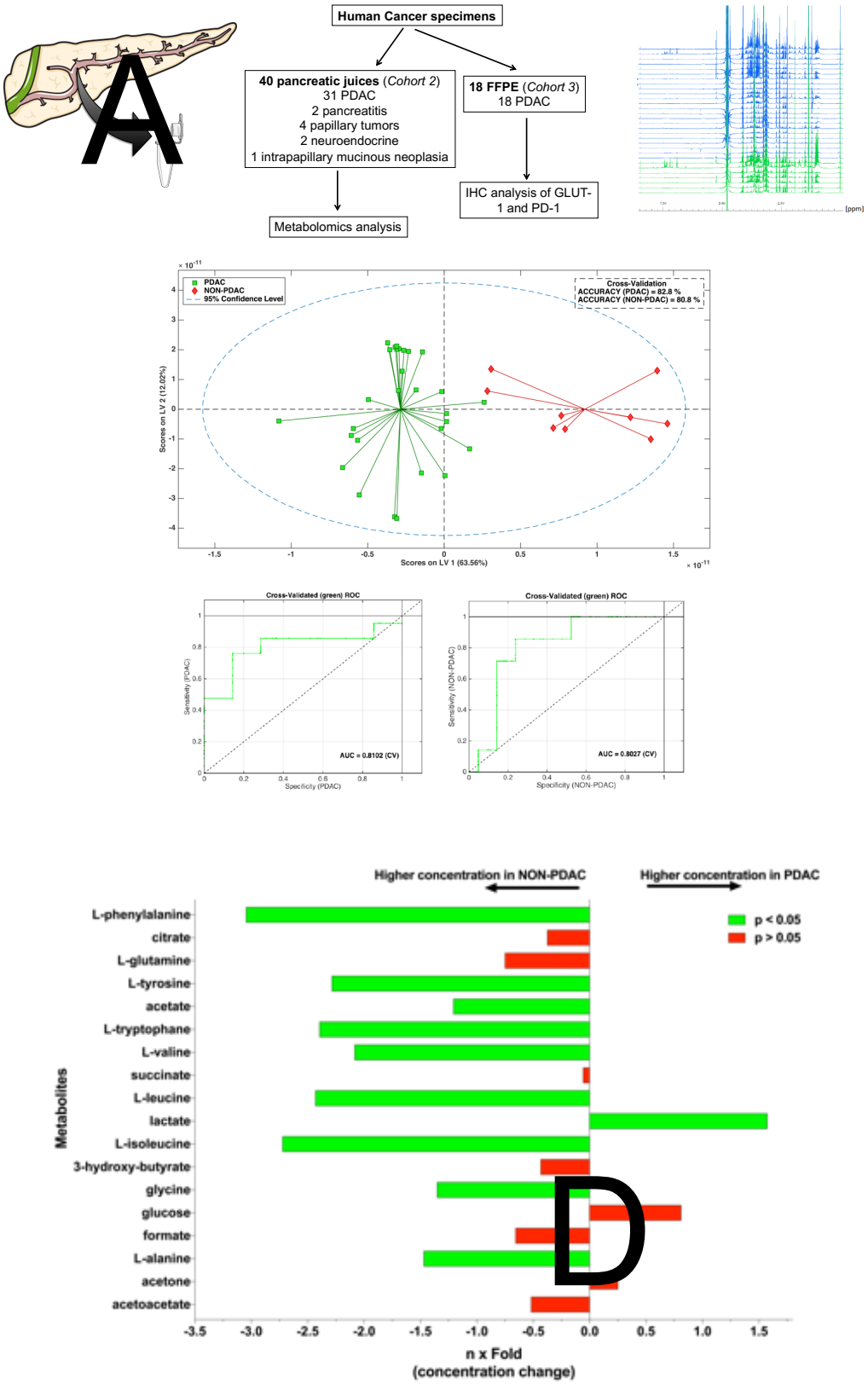

Figure 4.1. Metabolomic analysis of pancreatic juice. (**A**) Schematic representation depicting the secretion of pancreatic juice into the pancreatic duct and its collection during surgery. (**B**) Schematic description of the two cohorts of PDAC patients employed in the study. (**C**) 1H NMR CPMG spectra of PDAC samples (in blue) and non-PDAC samples (in

green) providing details on the small molecular weight metabolites contained in the pancreatic juices. (**D**) Supervised multivariate OPLS-DA analysis on CPMG spectra from PDAC samples (green squares) and non-PDAC samples (red diamonds) segregated the two groups (each one outlined by a spider plot), with an accuracy of 76% obtained by cross-validation. (**E**) ROC curves for the cross-validation of OPLS-DA analysis of PDAC (left) and non-PDAC (right). (**F**) "n Fold" concentration change calculated using the mean value of each metabolite in each group (PDAC vs non-PDAC). The integrals of metabolite signals have been normalized with total area of the spectra. The green bars indicate a p value < 0.05, and the red ones p > 0.05. Only lactate and glucose show a higher increased concentration trend in PDAC samples.

4.3 Glucose metabolism correlates with density of PD-1$^+$ cells in human and murine PDAC

We next considered whether the peculiar glucose metabolism observed in PDAC specimens correlated with specific immune profiles. Accelerated glucose metabolism in tumour cells (the so-called "Warburg effect") relies on modulation of key glycolytic enzymes, including the glucose transporter 1 (GLUT-1) [152]. To obtain a reliable indication of the Warburg effect in human PDAC tissues, I have analysed the expression of GLUT-1 in 18 PDAC specimens (**Figure 4.1, B**) by immunohistochemistry. Immunohistochemical staining evidenced a high degree of heterogeneity of GLUT-1 expression among pancreatic ducts, ranging from low (**Figure 4.2, A**) to very high positivity (**Figure 4.2, B**). Notably, GLUT-1 expression was higher in high-grade tumours (**Figure 4.2, C**), suggesting an association between a more aggressive phenotype and a higher glycolytic activity of pancreatic tumour cells. Then, to analyse how the tumour metabolic status correlates with the immune contexture in human PDAC, I have investigated potential associations of GLUT-1 expression with the presence of tumour-infiltrating leukocyte populations. By immunohistochemistry, the density (immunoreactive area (IRA%)) of GLUT-1 and of immune cells, including PD-1$^+$ cells (PD1-TILs, although it is impossible to unambiguously show that every PD1+ cell is a lymphocyte by imunohistochemistry), CD8$^+$ tumour-infiltrating lymphocytes (CD8-TILs), CD20$^+$ B lymphocytes (CD20-TILs), and CD68$^+$ tumour-associated macrophages (CD68-TAMs), were quantified (**Figure 4.3, A-D**). Intriguingly, the density of PD-1-TILs in 18 PDAC specimens correlated with the expression of GLUT-1 by

PDAC tumour cells (r=0.52, P=0.023) and notably, PD1-TILs were the only immune cells that showed a significant correlation with the expression of GLUT-1 (**Figure 4.3, E-H**). Moreover I have confirmed this immune-metabolic link in the Pdx1-Cre;Kras^{LSLG12D} genetic preclinical model of PDAC. While very low or absent expression of GLUT-1 was detected in the pancreas of wild-type (WT) mice (**Figure 4.4, A left**), weak to very intense immunoreactivity was present in the pancreatic tumours of Pdx1-Cre;Kras^{LSLG12D} mice (**Figure 4.4, A right**). An analogous expression pattern was shown by PD1-TILs (**Figure 4.4, B**) and, consistent with human PDAC, a positive correlation between GLUT-1 expression and PD1-TIL density was present (r=0.79, P=0.0007) (**Figure 4.4, C**).

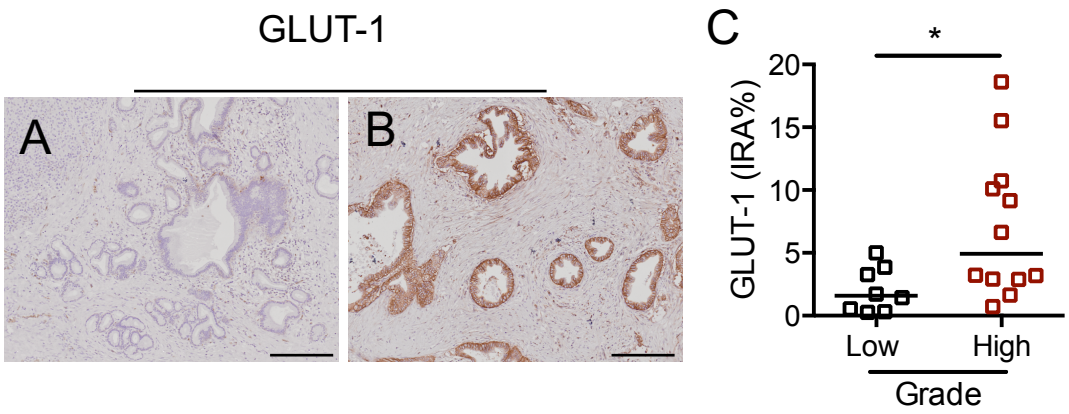

Figure 4.2. Immunohistochemical evaluation of GLUT-1 on PDAC paraffin sections. (**A-B**) Two representative specimens with low (**A**) and high (**B**) marker expression are shown. (**C**) Distribution of GLUT-1 expression (IRA%) according to tumour grade in 18 PDAC patients. Scale bars: 500μm. Black lines in the graph represent median.

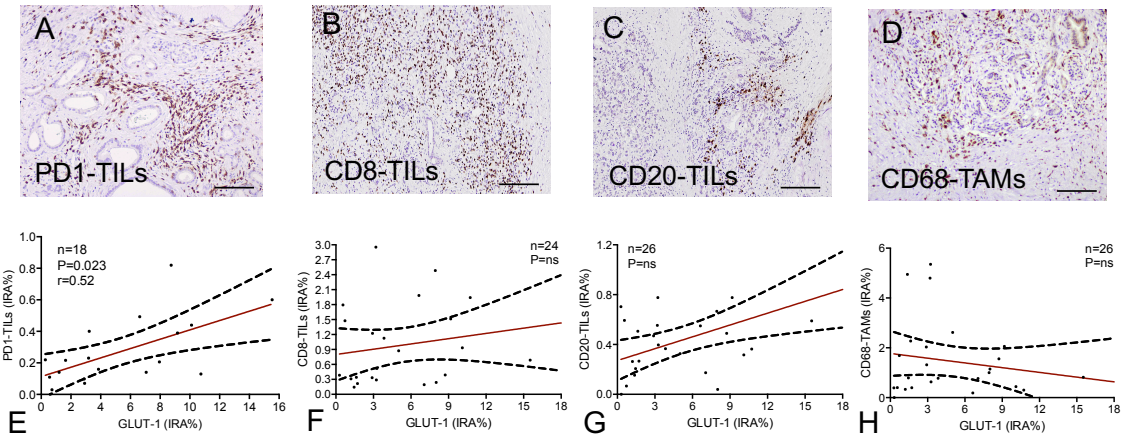

Figure 4.3. Immune variables in human PDAC specimens and their correlation with GLUT-1 expression. (**A-D**) Representative histological sections of human PDAC, stained for PD1-TILs (**A**), CD8-TILs (**B**), CD20-TILs (**C**) and CD68-TAMs (**D**). (**E-H**) Correlation of CD8-TILs (**E**), CD20-TILs (**F**), CD68-TAMs (**G**) and PD1-TILs (**H**) IRA% with GLUT-1 IRA%. P-value by Spearman's simple linear regression analysis (**E-H**). Bars: 500μm (**E-H**)

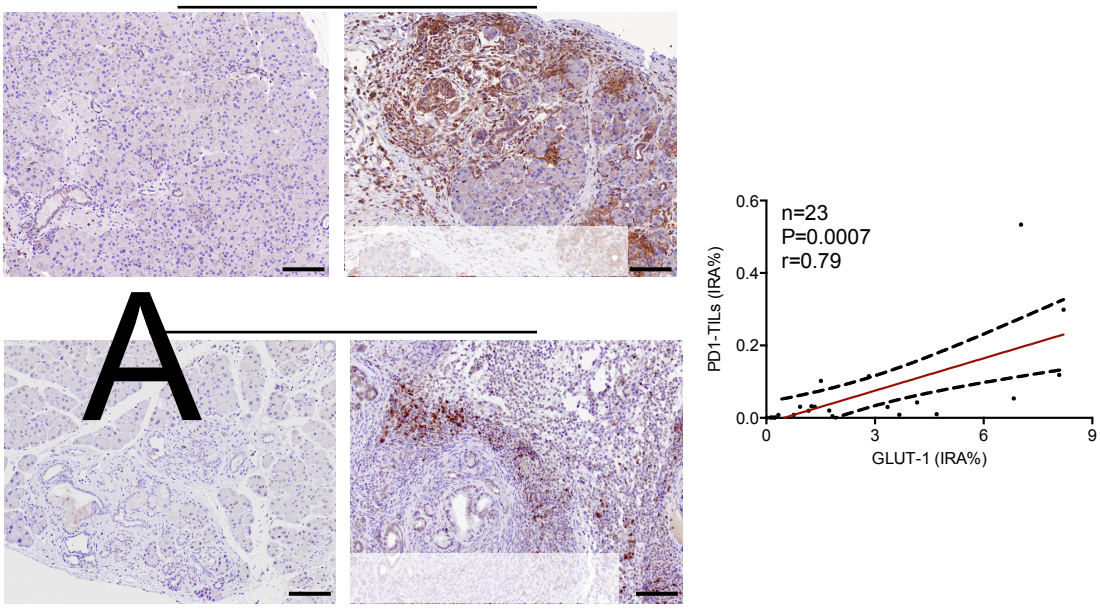

Figure 4.4. Correlation of Glut-1 and PD-1 expression in Kras-driven preclinical model of PDAC. Histological sections of pancreata of wild-type mice (**left)** and Pdx1-Cre;$Kras^{G12D}$ mice (**right**), stained with an anti-GLUT-1 (**A**) or anti-PD-1 (**B**) antibody. (**C**) Quantitative evaluation of the immunoreactive area (IRA%) reveals a linear correlation between the density of GLUT-1 and PD-1 in murine PDAC specimens (r=0.79, p=0.0007, n=23). P-value by Spearman's simple linear regression analysis in (**C**). Bars: 500μm (**A** and **B**).

4.4 Glucose uptake correlates with PD-1⁺ cells in preclinical models of PDAC

To further investigate the association between the tumour metabolic state and PD1-TIL infiltration and to characterize the PD-1⁺ cells in the tumour microenvironment, I have analysed implanted tumours obtained from two different pancreatic cell lines displaying different glucose uptake. DT6606 and Panc-02 are cell lines derived respectively from early and late stage murine PDAC (see methods "*PDAC preclinical models*") and were chosen on the basis of their glucose uptake, measured by *in vitro* accumulation of a fluorescent

WT

PD1-T

B

analogue of glucose (2NBDG) (**Figure 4.5, A**). Cells were incubated with 2NBDG, and representative images were collected by inverted fluorescence microscope to measure 2NBDG fluorescent signal (**Figure 4.5, B**). This analysis revealed that Panc02 cell line showed a significantly higher accumulation of 2NBDG compared to DT6606. On this premise I have subcutaneously injected DT6606 and Panc02 cell lines in mice, in order to test if the differential glucose accumulation rate was maintained after *in vivo* growth, and to characterize the phenotype of tumour infiltrating T cells in DT6606 and Panc02 derived tumours (**Figure 4.5, C**). Tumours obtained from the two tumour cell lines were not significantly different in size (**Figure 4.5, D**). The increased capability of accumulating glucose of Panc02 cells was retained after 3 weeks of growth *in vivo*, as measured by *ex vivo* imaging after injection of the fluorescent probe deoxy-D-glucose (2-DG-750). Analysis of 2-DG-750 fluorescence was performed on the excised tumour mass (**Figure 4.5, E**), to avoid confounding signals from surrounding tissues and revealed that Panc02 tumours up took significantly more glucose than DT6606 tumours (**Figure 4.5, F**). Consistent with the correlation between GLUT-1 expression and PD-1$^+$ T cell infiltrate observed in both human and murine PDAC (**Figure 4.3 and 4.4**), Panc02 tumours contained a higher percentage of PD1$^+$ cells within CD8$^+$ lymphocytes compared to DT6606 tumours (**Figure 4.6, A and B**), moreover CD8$^+$/PD1$^+$ T cells showed a significant increase in PD1-MFI (Mean Fluorescence Intensity) meaning that both the frequency of PD1$^+$ cells (**Figure 4.6, B**) and the expression of this receptor (**Figure 4.6, C**) were increased in Panc02 tumours. Remarkably, this difference was not a general feature of immune infiltrating cells, since the percentage of CD3$^+$ and CD8$^+$ cells was similar in DT6606 and Panc02 tumours (**Figure 4.6, D**), highlighting a selective increase of PD1 expression in highly metabolic tumours. Moreover the accumulation of CD8$^+$/PD1$^+$ cells was a specific feature of tumour infiltrating cells. In fact I measured the expression of PD1 on T cells from the inguinal lymph nodes of naïve and tumour-bearing mice (draining lymph node) and I compared them to tumour infiltrating T

cells (TILs). While there was only a slight increase in $CD8^+/PD1^+$ cells in the tumour draining lymph nodes compared to lymph nodes from naïve mice, their percentage was markedly inferior to the percentage of $CD8^+/PD1^+$ TILs (**Figure 4.6, E-F**). This highlighted that PD1 upregulation on T cells is driven by environmental cues specifically found in the tumour tissue.

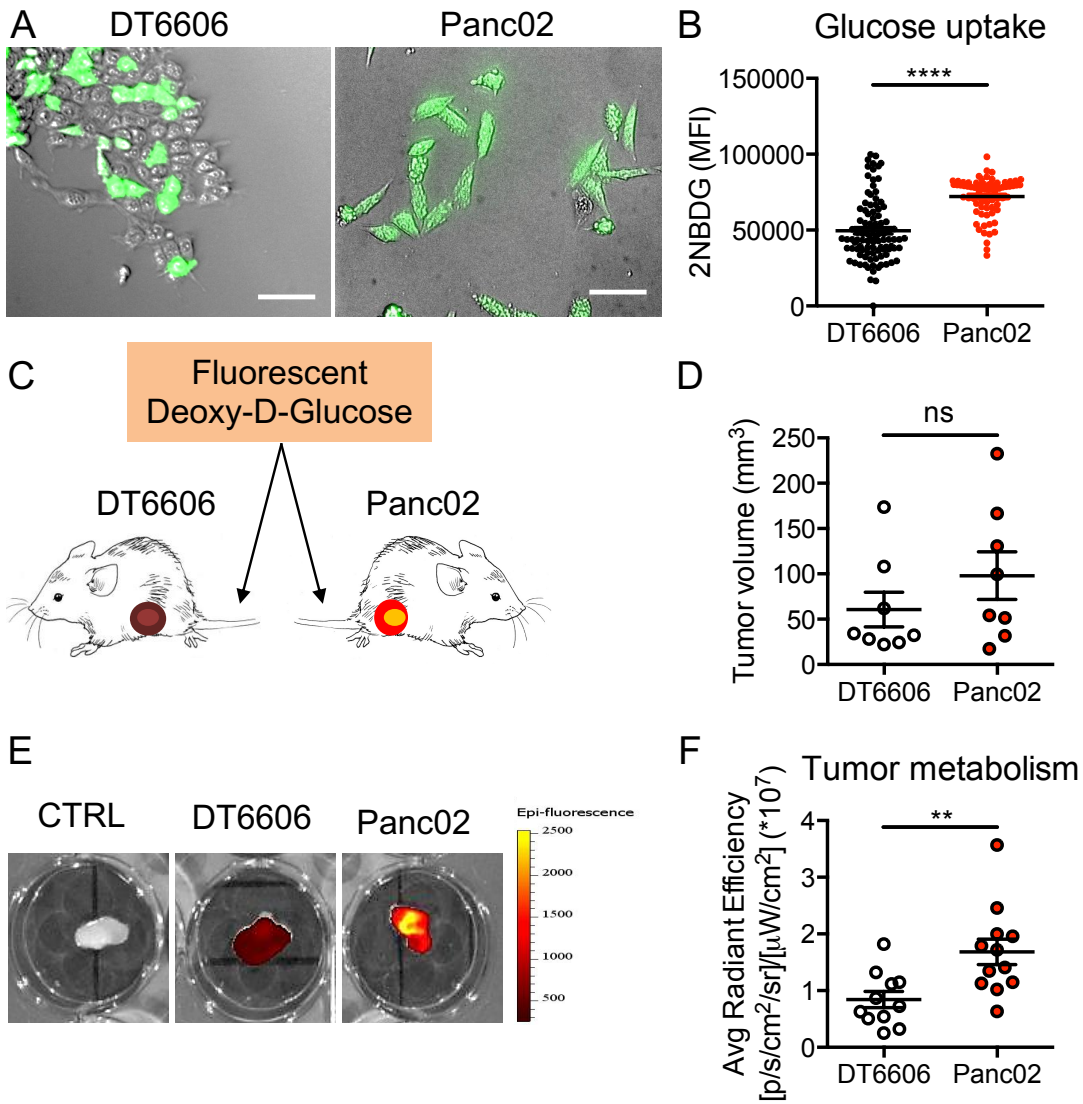

Figure 4.5. Glucose uptake characterization in implantable preclinical model of PDAC. *In vitro* fluorescence imaging of DT6606 and Panc02 exposed to 2NBDG, representative pics are reported (**A**). 2NBDG uptake by DT6606 and Panc02, Mean Fluorescent Intensity (MFI) is represented in the dot plot. Number of cells per replicate was at least 20 per group, mean values of three replicates are represented (**B**). Schematic representation of the PDAC preclinical model. DT6606 and Panc02 cell line are injected subcutaneously, and mice are sacrificed after 21 days from tumour cell injection. Tumour cells' glucose uptake measured after administration of the glucose fluorescent analogue 2DG-750 (Perkin Elmer) (**C**). Comparison of DT6606 (n=8) and Panc02 (n=7) tumour volume at sacrifice; one

representative experiment is shown (**D**). Representative tumours imaged *ex vivo* after i.v. injection of 2DG-750 (**E**). Measure of the Average Radiant Efficiency relative to 2DG-750 fluorescent signal in DT6606 (n=11) and Panc02 (n=12) tumours; graphs refer two independent experiments (**F**). Scale bars: 100µm (**A**); P-values are calculated by Mann-Whitney U-test (ns>0,05, **<0,01, ****<0,0001); black lines indicate mean, vertical bars represent SEM (**B, D** and **F**).

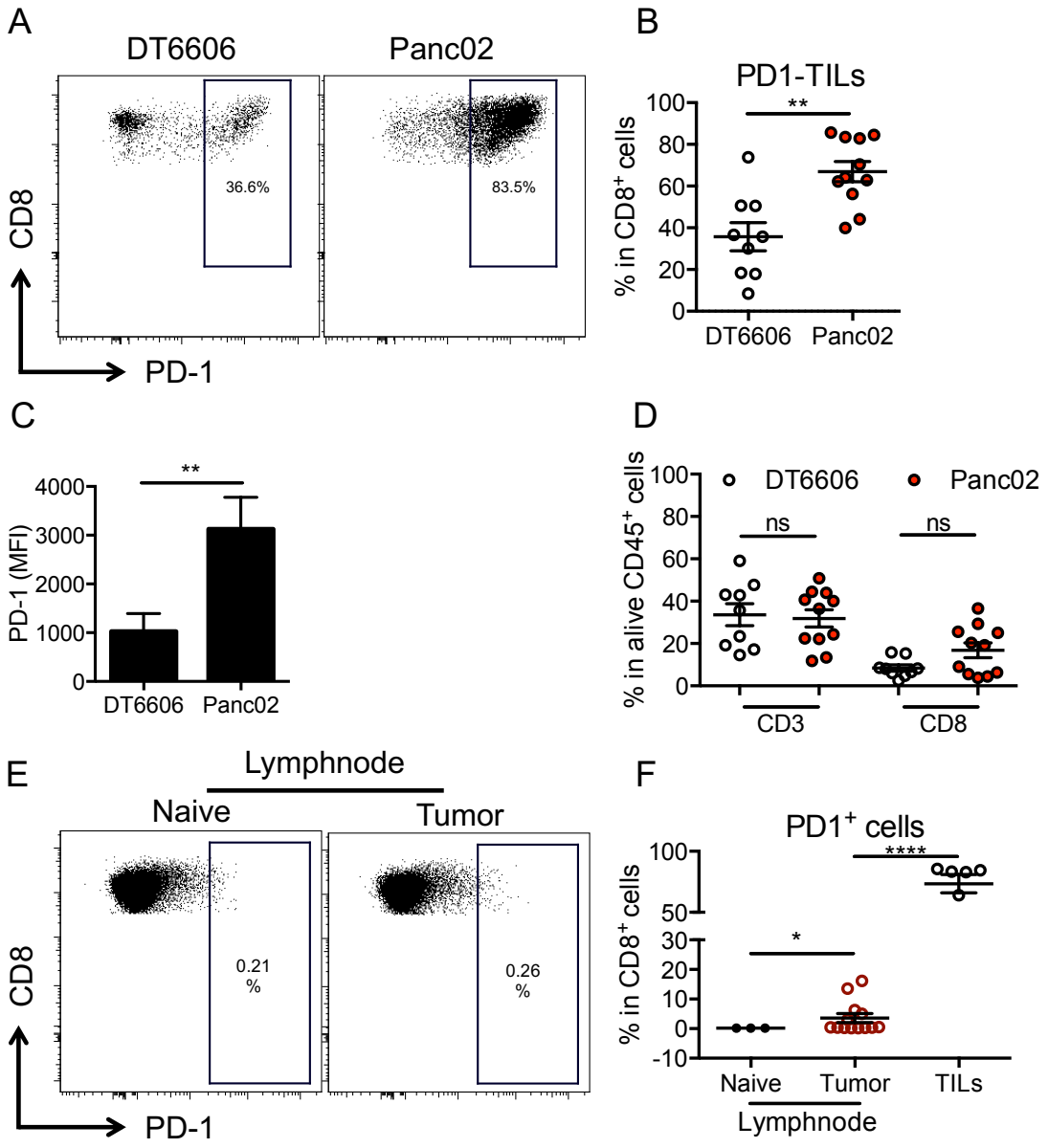

Figure 4.6. Expression of PD-1 on tumour infiltrating T cells in PDAC preclinical model. FACS dot plot showing PD-1 expression on $CD8^+$ TILs, from DT6606 and Panc02 tumours (**A**). Statistical analysis of PD-1 expression as percentage of $CD8^+$ T cells or as mean fluorescence intensity (**B** and **C** respectively). Frequency of $CD3^+$ or $CD8^+$ T cells as percentage of $CD45^+$ TILs in DT6606 and Panc02 tumours (**D**). FACS dot plot of lymph nodal $CD8^+$ T cells from inguinal lymph nodes of naïve (left) or tumour-bearing mice (right) (**E**). Statistical analysis of CD8+/PD1+ T cells distribution in inguinal lymph nodes, of naïve or tumour bearing mice, or in tumours (**F**). Graphs refer to at least two independent experiments (DT6606 n=9; Panc02 n=11; Naïve lymphnode n=3); P-values are calculated

by Mann-Whitney U-test (ns>0,05, *<0,05, **<0,01, ****<0,0001); black lines indicate mean, vertical bars represent SEM (**B, C, D** and **F**).

4.5 Targeting of glycolysis impacts on the accumulation of PD1-TILs in PDAC tumours

To analyse whether the increased metabolism of Panc02 cells was sufficient to determine PD1-TIL accumulation, two different approaches were adopted in order to inhibit glycolysis in Panc02 cells (**Figure 4.7, A and 4.8, B**). Pharmacological inhibition of the Warburg effect was achieved by administering the glycolysis inhibitor 2-deoxy-glucose (2-DG) in drinking water, for 2 weeks (**Figure 4.7, A**). At sacrifice neither tumour volume nor the percentage of $CD3^+$ and $CD8^+$ lymphocytes (**Figure 4.7, B and C respectively**) was significantly affected by the 2DG treatment. In contrast, inhibition of the glycolytic pathway by 2-DG, was sufficient to significantly reduce PD1-TIL infiltration in Panc02 tumours (**Figure 4.7 D-E**). Moreover, PD-1 MFI relative to $CD8^+$ lymphocytes was significantly reduced after 2DG treatment (**Figure 4.7 F**), confirming a direct involvement of glucose metabolism in the regulation of PD-1 expression. Despite its use in clinical trials, the administration of a non-specific glycolysis inhibitor such as 2-DG, could also interfere with glucose metabolism in effector T cells, affecting both their life span and effector functions [123]. Thus, we evaluated genetic silencing of glycolysis in Panc02 cells, in order to blunt the glycolytic metabolism only of tumour and not of immune cells. Glycolytic enzymes and other markers related to metabolic consumption are reliable indicators of the metabolic state of tumour cells. In a preliminary analysis, I have assessed the expression of main glucose transporters, and rate-limiting glycolytic enzymes in Panc02 cells (**Figure 4.8, A**) and opted for phosphofructokinase-m (PFK-m). This enzyme synthetizes fructose-1,6-bisphosphate, the first intermediate of glucose exclusively involved in the glycolytic reaction. This could reduce potential alterations of other metabolic pathways interconnected with glycolysis, such as the pentose phosphate pathway involved in nucleotide biosynthesis. Panc02 cells stably knocked-down with a shRNA targeting PFK-m (shPFK) and the corresponding control cell line stably expressing

a scramble sequence (shSCR), were generated. After 10 days of puromycin selection, the Pfk-m transcript was measured in both sh-SCR and sh-PFK cell lines and the gene silencing in sh-PFK was 75% compared to sh-SCR tumours (2^{-DDCt}=0,25 arbitrary units) (**Figure 4.8, B**). The two cell lines were implanted in mice, to originate tumours with opposite glycolytic rates and tumour growth was monitored for 24 days post-injection (**Figure 4.8, C**). This was not sufficient to affect tumour growth, nor the percentage of tumour infiltrating $CD3^+$ and $CD8^+$ lymphocytes (**Figure 4.8, D and E respectively**). Notably, genetic targeting of glucose metabolism significantly reduced the frequency of PD1-TILs within $CD8^+$ cells infiltrating Panc02 tumours (**Figure 4.8, F**), ultimately confirming the link between glucose metabolism and $CD8^+/PD1^+$ T cell infiltration. This result also suggests that targeting of tumour metabolism could be evaluated as a strategy to impact on the type of immune infiltration.

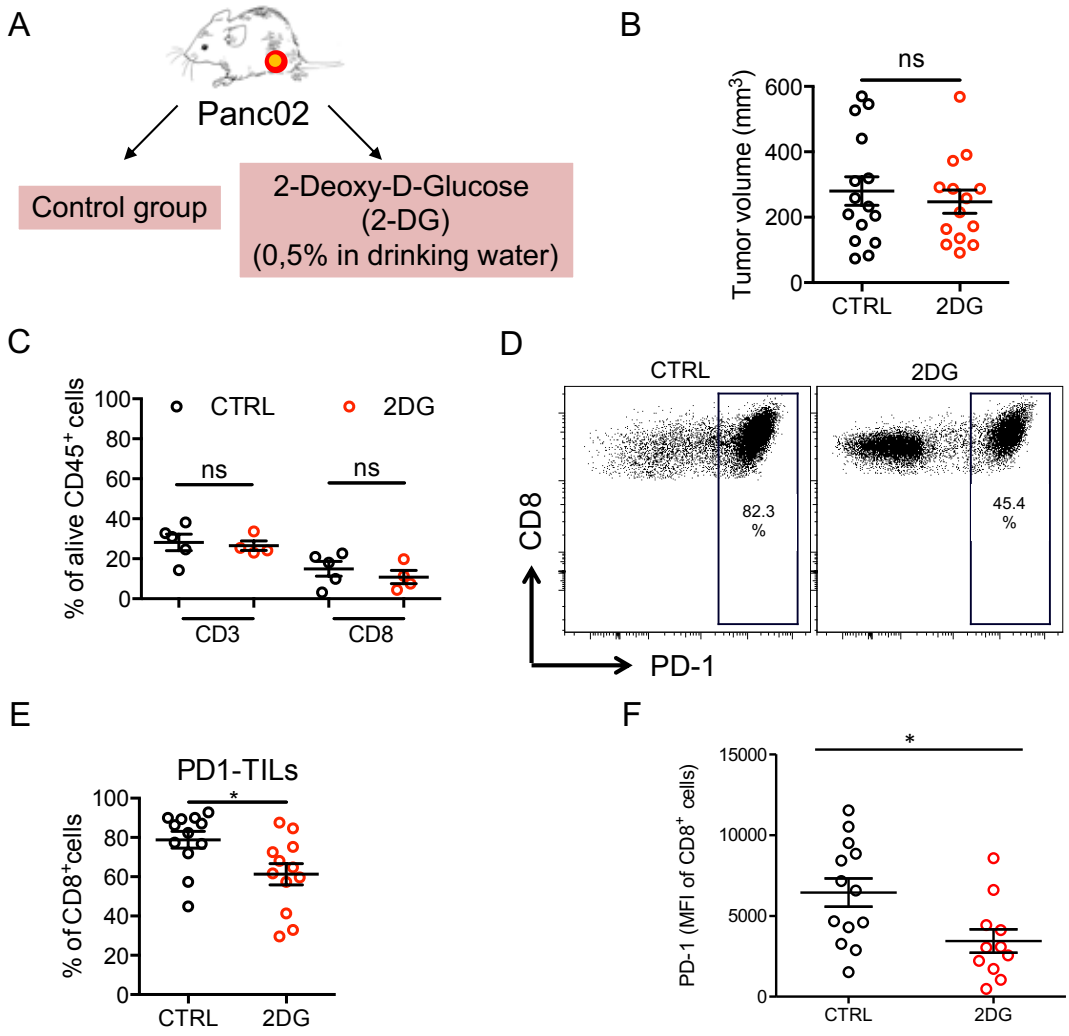

Figure 4.7 Pharmacological inhibition of glycolysis down-regulates PD-1 expression in tumour infiltrating CD8$^+$ T cells. Schematic representation of the experiment: seven days post subcutaneous injection of Panc02 cells, mice were treated with 0,5% 2-DG in drinking water or left untreated (**A**). Statistical analysis of tumour volume collected at sacrifice (CTRL n=15; 2DG n=14); two independent experiments are shown (**B**). Comparison of CD3$^+$ and CD8$^+$ TILs as percentage of CD45$^+$ cells between control (n=5) and treated (n=4) group; one representative experiment is shown (**C**). FACS dot plot of representative samples showing PD-1 expression on CD8$^+$ TILs in control and 2-DG treated mice (**D**) and relative statistical analysis of PD-1$^+$ cells percentage and PD-1 MFI (**E** and **F** respectively), both relative to CD8$^+$ TILs; two independent experiments are shown (CTRL n=12; 2DG n=12). P-values are calculated by Mann-Whitney U-test (ns>0,05, *<0,05); black lines indicate mean, vertical bars represent SEM (**B, C, E** and **F**).

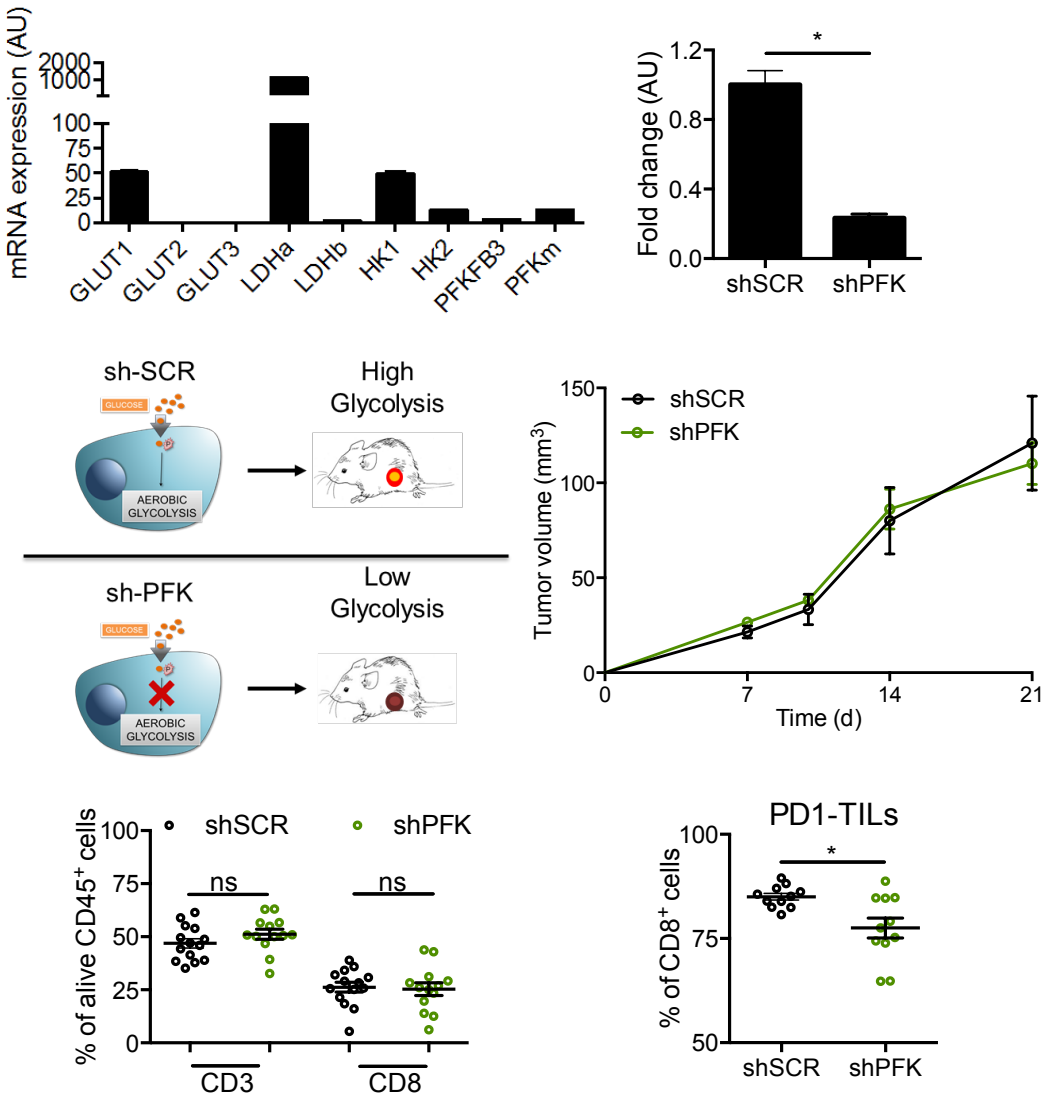

Figure 4.8 Genetic silencing of key glycolytic enzyme down-regulate PD-1 expression in tumour infiltrating CD8⁺ T cells. Preliminary analysis of genes encoding key glycolytic enzymes in Panc02 cell line (**A**). Semi quantitative RT-PCR to calculate gene silencing in sh-PFK cell line after two weeks of puromycin selection. The experiment was performed in triplicate, and graph shows fold change of Pfk-m transcript calculated as 2^{-DDCt}, where DDCt refers to mean DCt found in sh-SCR cell line (**B**). Schematic representation of the experiment: sh-SCR (high glycolysis) and sh-PFK (low glycolysis) cell lines were subcutaneously injected and tumour growth was allowed for 21 days post-injection (**C**). Tumour growth curve showing that sh-PFK tumours have the same progression of sh-SCR tumours *in vivo* (**D**). FACS analysis showing $CD3^+$ and $CD8^+$ T cells as percentage of CD45+ alive cells, and $PD1^+$ T cells as percentage of $CD8^+$ T cells in both sh-SCR and sh-PFK tumours (**E** and **F** respectively). **D** and **E**: n=14 (shSCR) and n=13 (shPFK), **F**: n=11 (shSCR) and n=11 (shPFK), two independent experiments are shown. P-values are calculated by Mann-Whitney U-test (ns>0,05, *<0,05); black lines indicate mean, vertical bars represent SEM (**B, E** and **F**).

C

4.6 Combinatorial targeting of glucose metabolism and PD-1/PD-L1 axis in vivo

To test whether modulation of the Warburg effect in Panc02 PFK-silenced cells was sufficient to determine a different responsiveness to anti-PD1 treatment, we administered the antibody twice a week until sacrifice to mice implanted with Panc02 shSCR or Panc02 shPFK (**Figure 4.9, A**). Tumour growth in tumours obtained from both shSCR and shPFK cells treated with anti-PD1 antibody was slower compared to mice treated with isotype control antibody, but the reduction in tumour growth after treatment was statistically significant only in shPFK tumours (**Figure 4.9, B**). This corresponded to a reduction in tumour mass at sacrifice (**Figure 4.9, C**). To further investigate metabolic reprogramming occurring in cancer cells after both Pfk-m silencing and anti-PD1 treatment, I isolated $CD45^+$ tumour infiltrating leukocytes ($CD45^+$ cells) from tumour and stromal $CD45^-$ cells at sacrifice, and evaluated the expression of genes encoding for glycolytic enzymes in $CD45^-$ cells. All genes that showed a significant modulation ($p<0,05$) between sh-PFK, treated or not with the anti-PD1 immunotherapy, and control groups were included in the heatmap (**Figure 4.9, D**). Surprisingly, I observed that in sh-PFK tumours, genes involved in glycolytic reactions up-stream to Pfk-m, including *Glut-1* (glucose transporter 1), *HK-2* (Hexokinase-2), and *Pfk-FB3* (phosphofructokinase-fructose bisphosphatase 3) were selectively down-regulated compared to both treated and untreated shSCR tumours. On the contrary, genes responsible of glycolytic reactions downstream of Pfk-m, *Eno1* (enolase 1), *PK-M1/2* (pyruvate kinase), *Pdk2* (pyruvate dehydrogenase kinase 2) and *Mct4* (monocarboxylate transporter 4), resulted significantly up-regulated in sh-PFK tumours. The up-regulation of glycolytic enzyme transcripts is frequently observed upon substrate restriction. This finding is in line with the assumption that Pfk-m knockdown caused a restriction in the availability of downstream glycolytic metabolites, thus confirming that glucose metabolism of sh-PFK tumours has been targeted and its alteration is maintained both after *in vivo* growth and after anti-PD1 immunotherapy. In order to explain the differential responsiveness to anti-PD1

treatment in our setting, the expression of the PD1 ligand (PD-L1) was measured, by semi quantitative RT-PCR, in all the cell lines used in our models. Surprisingly, the highest glycolytic cell line (Panc02-shSCR) showed the most abundant expression of PD-L1 mRNA compared to the lowest glycolytic cell line (DT6606), and accordingly, Pfk-m knock-down cells (Panc02-shPFK), with a reduced glycolytic activity, displayed an intermediate expression. This finding suggests a possible interconnection between glycolysis and the expression of the immune regulatory molecule PD-L1 (**Figure 4.9, E**).

Next we evaluated a panel of immune-related genes in $CD45^+$ cells, isolated from sh-PFK tumours treated with anti-PD1 antagonist and from their relative sh-SCR control tumours, by performing a gene expression array (RT^2 Profiler PCR Array, QIAGEN). Among the 84 genes analysed, those that presented a low modulation (p>0,05) comparing shPFK and shSCR $CD45^+$ cells, were excluded from the analysis. Significantly modulated genes (n=41) are reported in the heatmap (**Figure 4.9, F**), which has been calculated by hierarchical clustering of normalized gene expression (z-score). $CD45^+$ cells from shPFK and shSCR tumours segregated in two different clusters depending on their gene expression profile, suggesting that the modulation of immune-related genes mediated by the anti-PD1 immunotherapy is influenced by the metabolic state of tumour cells. In particular, the gene expression array revealed that comparing $CD45^+$ cells from shPFK and shSCR tumours, the anti-PD1 treatment up-regulated genes involved in antigen presentation (*HK2-K1 and H2-D1*), T and NK cell recruitment (*CXCL9, CCL4, CXCR4, CCR5*), inflammatory transcription factors (*NF-kB* and *STAT1*) and cytokines (*Tnf, IL12b, IL1a, IL1b*); concomitantly, $CD45^+$ cells from shPFK displayed a significant down-regulation of genes related to Th2/17 polarizing cytokines (*IL5, IL13, IL17a*) and T cell immunosuppression (*Ido1*). The gene expression analysis reveals that the metabolic background of tumour cells significantly impacts on the expression of immune-related genes by $CD45^+$-TILs upon anti-PD1 treatment. This supports the hypothesis that metabolic cues in the tumour microenviroment

need to be considered in order to maximize the anti-tumour immune response, beside the targeting of specific immunological pathways.

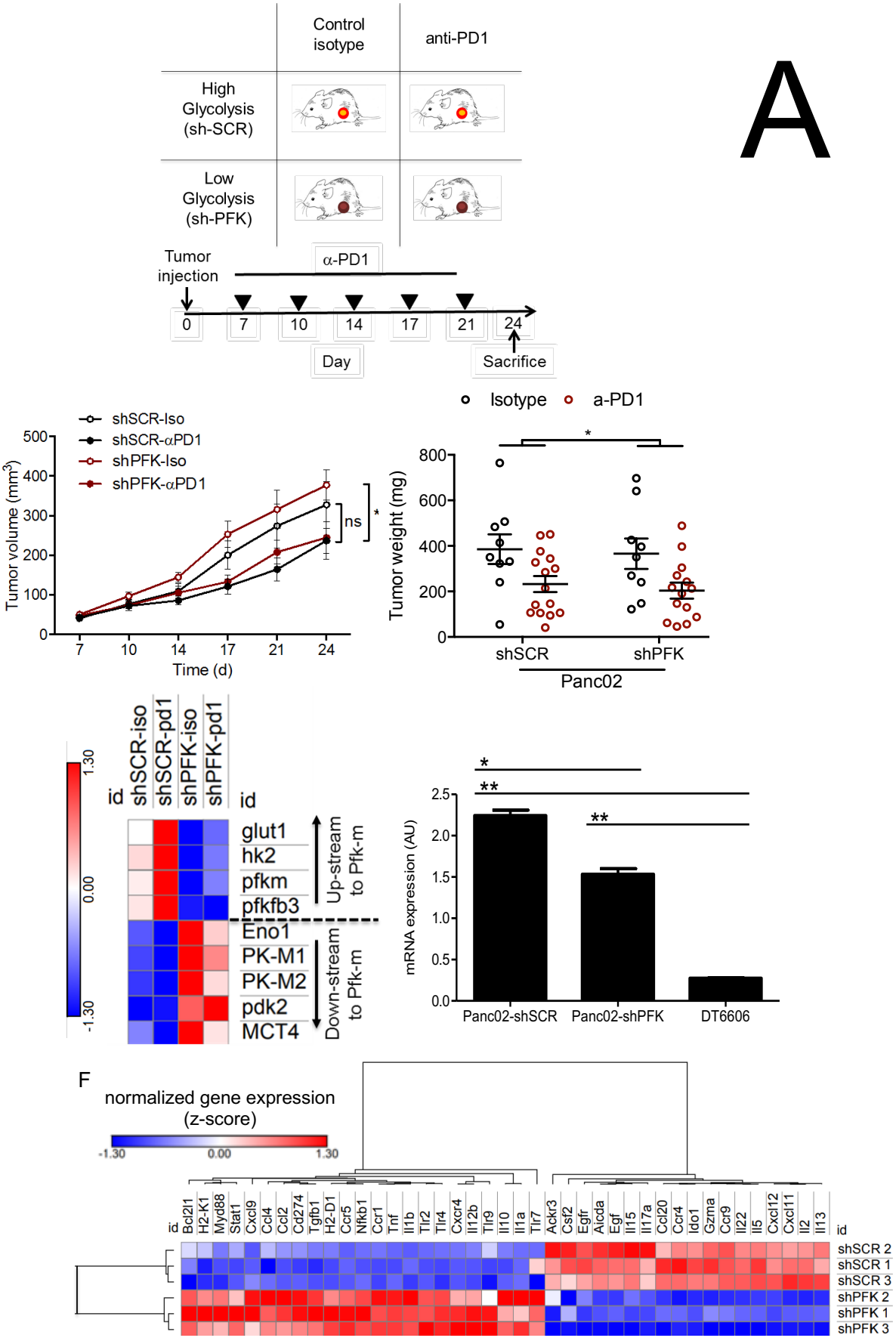

Figure 4.9 Interaction between tumour glycolysis and anti-PD1 immunotherapy. Schematic representation of the experiment: mice were subcutaneously injected with sh-SCR and sh-PFK tumour cell lines; 7 days post-injection mice were treated with 5 i.p.

injections of anti-PD1 or control isotype antibody, twice per week; 24 days post-injection mice were sacrificed and tumours collected (**A**). Tumour growth curve and tumour weight at sacrifice show the impact of anti-PD1 therapy on tumour progression in sh-SCR or sh-PFK tumours (**B** and **C** respectively). Heat map representing z-scores of significantly modulated genes in $CD45^-$ cells from sh-SCR and sh-PFK tumours treated with anti-PD1 or control isotype antibody (**D**). RT-PCR to evaluate the association between glycolysis and *Pdl1* mRNA expression, reported as arbitrary units (2^{-DCt}) (**E**). Hierarchical clustering of significantly modulated genes in three samples of $CD45^+$ cells from sh-SCR and sh-PFK tumours treated with anti-PD1 immunotherapy (**F**). (**B** and **C**) Graphs show means of at least two independent experiments; in the isotype-treated group n=9 in both shSCR and shPFK tumours, while in the anti-PD1 group n=15 in shSCR and n=14 in shPFK tumours; two-way ANOVA test was used and P values calculated by Tukey's multiple comparisons post-test (ns>0,05, *<0,05). (**E**) Graph shows means of two independent experiments and P-values are calculated by Mann-Whitney U-test (ns>0,05; *<0,05; **<0,01); dots (**B**), black lines (**C**), or bars (**E**) indicate mean, vertical bars represent SEM.

4.7 Discussion

The condition of nutrient deprivation frequently characterizes the tumour microenvironment. For this reason, a clear definition of tumour metabolic pathways can result in a better understanding of immune dysfunction in tumours.

We approached this issue by a metabolomics analysis in pancreatic juice, which allows us to appreciate the variety of molecules downstream relevant biological pathways. In pancreatic cancer, well-known for its metabolic alterations, metabolomics analyses of serum [154], urine [155] and even salivary fluids [156] have been performed and have led to relevant information, including discrimination of benign from malignant pancreatic diseases. However, pancreatic juice has been less explored for this purpose. Here pancreatic juice was collected intra-operatively. However, in a perspective of identifying early informative clinical markers, the collection of pancreatic juice could also be achieved by endoscopic ultrasound, retrograde cholangio-pancreatography or by endoscopic collection of duodenal juice secretion.

Multivariate statistical analysis of the NMR spectral data indicated significant group discrimination based on a disease-specific metabolic signature that singled out PDAC from other benign (pancreatitis) or less aggressive (papillary, neuroendocrine, IPMN) pancreatic pathological conditions. In particular, among 18 metabolites identified in pancreatic juice, only lactate exhibited a higher concentration in samples from PDAC patients, hinting to a specific alteration of glucose metabolism. A number of other metabolites were decreased in juices from PDAC patients, possibly suggesting the metabolic rewiring in favor of glycolysis. This comprehensive analysis, does not allow to investigate in detail the biochemical pathways ongoing in tumor cells, as it is the result of all the different cell types that contribute to the tumor metabolism, including stromal and immune cells. Nevertheless, the increased expression of the glucose transporter GLUT-1 in PDAC paraffin-embedded specimens

reflects an increased glucose uptake and further confirms a dis-regulated glucose metabolism, which, importantly, can be detected *in situ*, in pancreatic juice.

A better knowledge of the metabolic reprogramming characterizing tumors and how it impairs the function of immune cells could have an important impact on the design of immunotherapeutic strategies [148]. We have attempted to shed light on the immune-metabolic network by studying, in human PDAC specimens and *in vivo* preclinical models, how distinct tumor metabolisms correlate with the type of immune infiltration. Our data suggest that glucose metabolism is an important factor in the microenvironment of PDAC, by affecting the accumulation of $PD1^+$ cells in tumors. This result entails important clinical consequences. First, histo-pathological evaluation of the immune infiltrate, which is the dominant approach to grade the relevance of immune variables in cancer, only applies to surgical specimens, while a less invasive, pre-surgical identification of markers correlating with immune variables could represent a considerable advancement. Expression of PD-1 ligands in the tumor microenvironment has been validated as predictive biomarker of response to checkpoint inhibitors, with conflicting results [64]. Other mechanism-driven biomarker inquiries have shown that preexisting T-cell antitumor immunity is a prerequisite for increased susceptibility to immunomodulatory antibodies [157, 158]. Nonetheless, the mechanisms of resistance and variable response to checkpoint inhibitors remain poorly understood and suggest that factors other than the immunologic ones could emerge as important dictators of response to PD-1 targeted therapies.

On this line, attention has been turned to metabolic variables. In melanoma patients, baseline concentration of lactate dehydrogenase (LDH) measured in blood routine tests has been identified as a predictive biomarker of response to anti CTLA-4 treatment [93, 159, 160]. However, this marker is still not routinely used to influence therapeutic decisions,

possibly due to its rapid increase during stress responses. In [93] the authors suggested that LDH increase could mark the glycolytic switch of tumour cell metabolism, supporting the idea that the stimulatory effect of immunotherapy is dampened by the aberrant glucose metabolism in tumour microenvironment. Accordingly, we observed that targeting glycolysis significantly impacted the antitumor immune response mediated by anti-PD1 therapy. Although this synergism is reflected by the selective modulation of genes involved in antigen-specific immunity, the effect observed *in vivo* was only mild albeit significant. Being already measured in daily routine laboratory setting, the evaluation of LDH level could be easily translated to daily clinical practice. Interestingly, no mechanistic explanation for the predictive function of LDH levels to checkpoint inhibitors had been provided so far.
In the case of pancreatic adenocarcinoma, however, these issues are still out of reach. In fact, the nature of the intense stroma preventing recruitment of immune cells has represented an obstacle to the introduction of strategies targeting the immune system.

In this work, inhibition of glycolysis in tumor cells specifically affected PD1 expression in T cells, without impairing $CD8^+$ T cell recruitment, suggesting that the metabolic profile of tumor cells can modulate the immune response by shaping the phenotype of cytotoxic T cells. It is known in literature that unavailability of metabolic substrates for the glycolytic reaction can lead to immune dis-regulation and inappropriate immune responses. Essentially, distinct metabolic pathways characterize T cells according to their functional state in the course of immune responses. In the case of cytotoxic T cells, a remarkable feature is the considerable and sudden increase in glucose uptake following the immune stimulus and differentiation to cytolytic effectors [146, 147], a process required to switch from the oxidative phosphorylation pathway to the glycolytic one, necessary to sustain rapid cell growth. However, formal demonstration that nutrient deprivation modulates $PD1^+$ T cell frequency has not been provided yet. Alternatively to this “nutrient competition” scenario,

lactate and other metabolites are not only by-products of high-proliferating cells, but act as signaling molecules capable of negatively modulating immune cell functions [161-163]. Cell metabolism could have a role also in T cell exhaustion, a condition of unresponsiveness associated to chronic antigen stimulation, frequently observed during chronic infection and cancer [164, 165]. The PD-1-PD-L1 pathway, a prominent target in cancer immunotherapy, also induces metabolic reprogramming of T cell metabolism [166].

We also show an increased response to the anti-PD1 treatment in tumors metabolically re-educated by glycolysis inhibition, indicating that manipulation of tumor metabolism could also result in the reboot of T cell function. This also suggests that combinatorial strategies concomitantly targeting metabolism and checkpoint inhibitors could be evaluated in a therapeutic perspective. However, we have not formally proved that PD-1 positive cells are exhausted. Despite their common association to T-cell inhibition and immunosuppressive conditions, PD1 expressing tumor-infiltrating cells have been also shown to be a favorable prognostic marker in HPV^{+} head and neck cancer [167]. Moreover, in chronic infections, PD1 cells are the ones producing cytokines [168]. This controversial function of the PD1 molecule does not however contrast with the use of anti-checkpoint antibodies, which are supposed to act by blocking inhibitory signals engaging the PD1. Dysregulation in metabolic pathways could contribute to such inhibitory signals and, together with the possibility to synergize with other checkpoint inhibitors, need further investigation.

5. Concluding remarks

In this thesis I have summarized the main findings collected during my PhD training, which has been focused on relatively unexplored aspects of the immune infiltrate of pancreatic cancer. Pancreatic cancer is frequently reported as hypo-responsive to immunotherapeutic treatments, which have been little introduced for this tumour type, with a few exceptions (i.e. anti-CD40 and vaccination). During these years, I have nurtured the idea that the general view of pancreatic adenocarcinoma as a tumor environment hostile to immune infiltration could have hampered the introduction of immune-based approaches for this neoplastic disease. Based on my analyses and on the knowledge that I've acquired on the immune microenvironment of PDAC, a considerable number and types of immune cells populate pancreatic cancer tissues, suggesting that there is chance that targeting immune cells could result beneficial also for pancreatic cancer patients.

In the first part, I have introduced a relatively new component of the immune contexture of different tumours, namely tertiary lymphoid tissue. The occurrence of TLT in the tumour microenvironment has two important outcomes on the design of immunotherapeutic approaches. To begin with, the presence of a lymphoid site could favour recruitment of immune cells and their *in situ* activation, thus it could increase responsiveness to adoptive cell therapies. Moreover, my analysis focused on the B cell component and suggesting their dual function in tumours reinforces the hypothesis that B cell targeting could be effective also in solid tumours. Finally, immunotherapeutic vaccination protocols could boost the function of TLT, as I showed here and as it has been already shown in literature [42], thus it could benefit from a microenvironment conducive to TLT formation.

In the second part, my analysis of the intersection between tumour metabolism and PD-1+ cell infiltration suggests how a better knowledge of the metabolic reprogramming characterizing tumours and how it impairs the function of immune cells could have an important impact on the design of immunotherapeutic strategies. So far, the PD1-PDL1 axis has emerged as one of the most promising immunotherapeutic pathways already translated

into clinical practice. Surprisingly, however, the simple evaluation of the expression of such biomarkers has been reported as inaccurate in predicting therapy effectiveness [64]. Our data suggest that other factors, including metabolic variables could affect PD1 expression in T cells. We observed a significant tumour reduction upon anti-PD1 treatment only in tumours metabolically re-educated by glycolysis targeting. This indicates that manipulation of tumour metabolism could also result in the reboot of T cell function. This also suggests that combinatorial strategies concomitantly targeting metabolism and checkpoint inhibitors could be evaluated in a therapeutic perspective.

Bibliography

1. Hanahan, D. and R.A. Weinberg, *Hallmarks of cancer: the next generation.* Cell, 2011. **144**(5): p. 646-74.
2. Mantovani, A., et al., *Cancer-related inflammation.* Nature, 2008. **454**(7203): p. 436-44.
3. Schreiber, R.D., L.J. Old, and M.J. Smyth, *Cancer immunoediting: integrating immunity's roles in cancer suppression and promotion.* Science, 2011. **331**(6024): p. 1565-70.
4. Vesely, M.D., et al., *Natural innate and adaptive immunity to cancer.* Annu Rev Immunol, 2011. **29**: p. 235-71.
5. Gentles, A.J., et al., *The prognostic landscape of genes and infiltrating immune cells across human cancers.* Nat Med, 2015. **21**(8): p. 938-945.
6. Mantovani, A. and P. Allavena, *The interaction of anticancer therapies with tumor-associated macrophages.* J Exp Med, 2015. **212**(4): p. 435-45.
7. Shalapour, S. and M. Karin, *Immunity, inflammation, and cancer: an eternal fight between good and evil.* J Clin Invest, 2015. **125**(9): p. 3347-55.
8. Shankaran, V., et al., *IFNgamma and lymphocytes prevent primary tumour development and shape tumour immunogenicity.* Nature, 2001. **410**(6832): p. 1107-11.
9. Mlecnik, B., et al., *Tumor immunosurveillance in human cancers.* Cancer Metastasis Rev, 2011. **30**(1): p. 5-12.
10. Gajewski, T.F., H. Schreiber, and Y.X. Fu, *Innate and adaptive immune cells in the tumor microenvironment.* Nat Immunol, 2013. **14**(10): p. 1014-22.
11. Smyth, M.J., et al., *Perforin-mediated cytotoxicity is critical for surveillance of spontaneous lymphoma.* J Exp Med, 2000. **192**(5): p. 755-60.
12. Street, S.E., et al., *Suppression of lymphoma and epithelial malignancies effected by interferon gamma.* J Exp Med, 2002. **196**(1): p. 129-34.
13. Davidson, W.F., T. Giese, and T.N. Fredrickson, *Spontaneous development of plasmacytoid tumors in mice with defective Fas-Fas ligand interactions.* J Exp Med, 1998. **187**(11): p. 1825-38.
14. Boshoff, C. and R. Weiss, *AIDS-related malignancies.* Nat Rev Cancer, 2002. **2**(5): p. 373-82.
15. Frisch, M., et al., *Association of cancer with AIDS-related immunosuppression in adults.* JAMA, 2001. **285**(13): p. 1736-45.
16. Kirk, G.D., et al., *HIV infection is associated with an increased risk for lung cancer, independent of smoking.* Clin Infect Dis, 2007. **45**(1): p. 103-10.
17. Olalekan, S.A., et al., *B cells expressing IFN-gamma suppress Treg-cell differentiation and promote autoimmune experimental arthritis.* Eur J Immunol, 2015. **45**(4): p. 988-98.
18. Hu, C.Y., et al., *Treatment with CD20-specific antibody prevents and reverses autoimmune diabetes in mice.* J Clin Invest, 2007. **117**(12): p. 3857-67.
19. Bouaziz, J.D., et al., *Therapeutic B cell depletion impairs adaptive and autoreactive CD4+ T cell activation in mice.* Proc Natl Acad Sci U S A, 2007. **104**(52): p. 20878-83.
20. Lund, F.E., *Cytokine-producing B lymphocytes-key regulators of immunity.* Curr Opin Immunol, 2008. **20**(3): p. 332-8.
21. Crawford, A., et al., *Primary T cell expansion and differentiation in vivo requires antigen presentation by B cells.* J Immunol, 2006. **176**(6): p. 3498-506.
22. Maletzki, C., et al., *Ex-vivo clonally expanded B lymphocytes infiltrating colorectal carcinoma are of mature immunophenotype and produce functional IgG.* PLoS One, 2012. **7**(2): p. e32639.
23. Nielsen, J.S., et al., *CD20+ tumor-infiltrating lymphocytes have an atypical CD27- memory phenotype and together with CD8+ T cells promote favorable prognosis in ovarian cancer.* Clin Cancer Res, 2012. **18**(12): p. 3281-92.

24. Shi, J.Y., et al., *Margin-infiltrating CD20(+) B cells display an atypical memory phenotype and correlate with favorable prognosis in hepatocellular carcinoma.* Clin Cancer Res, 2013. **19**(21): p. 5994-6005.
25. Ahmadi, T., et al., *CD40 Ligand-activated, antigen-specific B cells are comparable to mature dendritic cells in presenting protein antigens and major histocompatibility complex class I- and class II-binding peptides.* Immunology, 2008. **124**(1): p. 129-40.
26. Gnjatic, S., et al., *Cross-presentation of HLA class I epitopes from exogenous NY-ESO-1 polypeptides by nonprofessional APCs.* J Immunol, 2003. **170**(3): p. 1191-6.
27. Rodriguez-Pinto, D., *B cells as antigen presenting cells.* Cell Immunol, 2005. **238**(2): p. 67-75.
28. Nelson, B.H., *CD20+ B cells: the other tumor-infiltrating lymphocytes.* J Immunol, 2010. **185**(9): p. 4977-82.
29. Al-Shibli, K.I., et al., *Prognostic effect of epithelial and stromal lymphocyte infiltration in non-small cell lung cancer.* Clin Cancer Res, 2008. **14**(16): p. 5220-7.
30. Nedergaard, B.S., et al., *A comparative study of the cellular immune response in patients with stage IB cervical squamous cell carcinoma. Low numbers of several immune cell subtypes are strongly associated with relapse of disease within 5 years.* Gynecol Oncol, 2008. **108**(1): p. 106-11.
31. Lundgren, S., et al., *Prognostic impact of tumour-associated B cells and plasma cells in epithelial ovarian cancer.* J Ovarian Res, 2016. **9**: p. 21.
32. Kornbluth, R.S., M. Stempniak, and G.W. Stone, *Design of CD40 agonists and their use in growing B cells for cancer immunotherapy.* Int Rev Immunol, 2012. **31**(4): p. 279-88.
33. Silina, K., et al., *Manipulation of tumour-infiltrating B cells and tertiary lymphoid structures: a novel anti-cancer treatment avenue?* Cancer Immunol Immunother, 2014. **63**(7): p. 643-62.
34. Aloisi, F. and R. Pujol-Borrell, *Lymphoid neogenesis in chronic inflammatory diseases.* Nat Rev Immunol, 2006. **6**(3): p. 205-17.
35. Carragher, D.M., et al., *A novel role for non-neutralizing antibodies against nucleoprotein in facilitating resistance to influenza virus.* J Immunol, 2008. **181**(6): p. 4168-76.
36. Neyt, K., et al., *Tertiary lymphoid organs in infection and autoimmunity.* Trends Immunol, 2012. **33**(6): p. 297-305.
37. Dieu-Nosjean, M.C., et al., *Tertiary lymphoid structures in cancer and beyond.* Trends Immunol, 2014. **35**(11): p. 571-80.
38. Pitzalis, C., et al., *Ectopic lymphoid-like structures in infection, cancer and autoimmunity.* Nat Rev Immunol, 2014. **14**(7): p. 447-62.
39. Moyron-Quiroz, J.E., et al., *Role of inducible bronchus associated lymphoid tissue (iBALT) in respiratory immunity.* Nat Med, 2004. **10**(9): p. 927-34.
40. de Chaisemartin, L., et al., *Characterization of chemokines and adhesion molecules associated with T cell presence in tertiary lymphoid structures in human lung cancer.* Cancer Res, 2011. **71**(20): p. 6391-9.
41. Di Caro, G. and F. Marchesi, *Tertiary lymphoid tissue: A gateway for T cells in the tumor microenvironment.* Oncoimmunology, 2014. **3**: p. e28850.
42. Lutz, E.R., et al., *Immunotherapy converts nonimmunogenic pancreatic tumors into immunogenic foci of immune regulation.* Cancer Immunol Res, 2014. **2**(7): p. 616-31.
43. Murakami, J., et al., *Functional B-cell response in intrahepatic lymphoid follicles in chronic hepatitis C.* Hepatology, 1999. **30**(1): p. 143-50.
44. Armengol, M.P., et al., *Thyroid autoimmune disease: demonstration of thyroid antigen-specific B cells and recombination-activating gene expression in chemokine-containing active intrathyroidal germinal centers.* Am J Pathol, 2001. **159**(3): p. 861-73.

45. Manzo, A., et al., *Secondary and ectopic lymphoid tissue responses in rheumatoid arthritis: from inflammation to autoimmunity and tissue damage/remodeling.* Immunol Rev, 2010. **233**(1): p. 267-85.
46. Di Caro, G., et al., *Tertiary lymphoid tissue in the tumor microenvironment: from its occurrence to immunotherapeutic implications.* Int Rev Immunol, 2015. **34**(2): p. 123-33.
47. Dieu-Nosjean, M.C., et al., *Long-term survival for patients with non-small-cell lung cancer with intratumoral lymphoid structures.* J Clin Oncol, 2008. **26**(27): p. 4410-7.
48. Cipponi, A., et al., *Neogenesis of lymphoid structures and antibody responses occur in human melanoma metastases.* Cancer Res, 2012. **72**(16): p. 3997-4007.
49. Coppola, D., et al., *Unique ectopic lymph node-like structures present in human primary colorectal carcinoma are identified by immune gene array profiling.* Am J Pathol, 2011. **179**(1): p. 37-45.
50. Bergomas, F., et al., *Tertiary intratumor lymphoid tissue in colo-rectal cancer.* Cancers (Basel), 2011. **4**(1): p. 1-10.
51. Martinet, L., et al., *Human solid tumors contain high endothelial venules: association with T- and B-lymphocyte infiltration and favorable prognosis in breast cancer.* Cancer Res, 2011. **71**(17): p. 5678-87.
52. Goc, J., et al., *Characteristics of tertiary lymphoid structures in primary cancers.* Oncoimmunology, 2013. **2**(12): p. e26836.
53. Finkin, S., et al., *Ectopic lymphoid structures function as microniches for tumor progenitor cells in hepatocellular carcinoma.* Nat Immunol, 2015. **16**(12): p. 1235-44.
54. Galluzzi, L., G. Kroemer, and A. Eggermont, *Novel immune checkpoint blocker approved for the treatment of advanced melanoma.* Oncoimmunology, 2014. **3**(11): p. e967147.
55. Lesterhuis, W.J., J.B. Haanen, and C.J. Punt, *Cancer immunotherapy--revisited.* Nat Rev Drug Discov, 2011. **10**(8): p. 591-600.
56. Smyth, M.J., et al., *Combination cancer immunotherapies tailored to the tumour microenvironment.* Nat Rev Clin Oncol, 2016. **13**(3): p. 143-58.
57. Kroemer, G., et al., *Natural and therapy-induced immunosurveillance in breast cancer.* Nat Med, 2015. **21**(10): p. 1128-38.
58. Marabondo, S. and H.L. Kaufman, *High-dose interleukin-2 (IL-2) for the treatment of melanoma: safety considerations and future directions.* Expert Opin Drug Saf, 2017. **16**(12): p. 1347-1357.
59. Kirkwood, J.M., G.D. Resnick, and B.F. Cole, *Efficacy, safety, and risk-benefit analysis of adjuvant interferon alfa-2b in melanoma.* Semin Oncol, 1997. **24**(1 Suppl 4): p. S16-23.
60. Anderson, P., M. Hoglund, and S. Rodjer, *Pulmonary side effects of interferon-alpha therapy in patients with hematological malignancies.* Am J Hematol, 2003. **73**(1): p. 54-8.
61. Pol, J., et al., *Trial Watch: Peptide-based anticancer vaccines.* Oncoimmunology, 2015. **4**(4): p. e974411.
62. Garg, A.D., et al., *Trial watch: Dendritic cell-based anticancer immunotherapy.* Oncoimmunology, 2017. **6**(7): p. e1328341.
63. Fournier, C., et al., *Trial Watch: Adoptively transferred cells for anticancer immunotherapy.* Oncoimmunology, 2017. **6**(11): p. e1363139.
64. Topalian, S.L., et al., *Mechanism-driven biomarkers to guide immune checkpoint blockade in cancer therapy.* Nat Rev Cancer, 2016. **16**(5): p. 275-87.
65. Topalian, S.L., et al., *Survival, durable tumor remission, and long-term safety in patients with advanced melanoma receiving nivolumab.* J Clin Oncol, 2014. **32**(10): p. 1020-30.
66. Motzer, R.J., et al., *Nivolumab for Metastatic Renal Cell Carcinoma: Results of a Randomized Phase II Trial.* J Clin Oncol, 2015. **33**(13): p. 1430-7.
67. Borghaei, H., et al., *Nivolumab versus Docetaxel in Advanced Nonsquamous Non-Small-Cell Lung Cancer.* N Engl J Med, 2015. **373**(17): p. 1627-39.

68. Galon, J., et al., *Towards the introduction of the 'Immunoscore' in the classification of malignant tumours.* J Pathol, 2014. **232**(2): p. 199-209.
69. Fridman, W.H., et al., *The immune contexture in human tumours: impact on clinical outcome.* Nat Rev Cancer, 2012. **12**(4): p. 298-306.
70. Galon, J., et al., *Cancer classification using the Immunoscore: a worldwide task force.* J Transl Med, 2012. **10**: p. 205.
71. Restifo, N.P., *A "big data" view of the tumor "immunome".* Immunity, 2013. **39**(4): p. 631-2.
72. Bindea, G., et al., *Spatiotemporal dynamics of intratumoral immune cells reveal the immune landscape in human cancer.* Immunity, 2013. **39**(4): p. 782-95.
73. Fridman, W.H., et al., *The immune contexture in cancer prognosis and treatment.* Nat Rev Clin Oncol, 2017. **14**(12): p. 717-734.
74. Bardeesy, N. and R.A. DePinho, *Pancreatic cancer biology and genetics.* Nat Rev Cancer, 2002. **2**(12): p. 897-909.
75. Siegel, R.L., K.D. Miller, and A. Jemal, *Cancer statistics, 2018.* CA Cancer J Clin, 2018. **68**(1): p. 7-30.
76. Clark, C.E., et al., *Dynamics of the immune reaction to pancreatic cancer from inception to invasion.* Cancer Res, 2007. **67**(19): p. 9518-27.
77. Ino, Y., et al., *Immune cell infiltration as an indicator of the immune microenvironment of pancreatic cancer.* Br J Cancer, 2013. **108**(4): p. 914-23.
78. Kurahara, H., et al., *Significance of M2-polarized tumor-associated macrophage in pancreatic cancer.* J Surg Res, 2011. **167**(2): p. e211-9.
79. Bayne, L.J., et al., *Tumor-derived granulocyte-macrophage colony-stimulating factor regulates myeloid inflammation and T cell immunity in pancreatic cancer.* Cancer Cell, 2012. **21**(6): p. 822-35.
80. Pylayeva-Gupta, Y., et al., *Oncogenic Kras-induced GM-CSF production promotes the development of pancreatic neoplasia.* Cancer Cell, 2012. **21**(6): p. 836-47.
81. Hiraoka, N., et al., *Prevalence of FOXP3+ regulatory T cells increases during the progression of pancreatic ductal adenocarcinoma and its premalignant lesions.* Clin Cancer Res, 2006. **12**(18): p. 5423-34.
82. Zheng, L., et al., *Role of immune cells and immune-based therapies in pancreatitis and pancreatic ductal adenocarcinoma.* Gastroenterology, 2013. **144**(6): p. 1230-40.
83. Soares, K.C., et al., *PD-1/PD-L1 blockade together with vaccine therapy facilitates effector T-cell infiltration into pancreatic tumors.* J Immunother, 2015. **38**(1): p. 1-11.
84. Winograd, R., et al., *Induction of T-cell Immunity Overcomes Complete Resistance to PD-1 and CTLA-4 Blockade and Improves Survival in Pancreatic Carcinoma.* Cancer Immunol Res, 2015. **3**(4): p. 399-411.
85. Carstens, J.L., et al., *Spatial computation of intratumoral T cells correlates with survival of patients with pancreatic cancer.* Nat Commun, 2017. **8**: p. 15095.
86. Erkan, M., et al., *The role of stroma in pancreatic cancer: diagnostic and therapeutic implications.* Nat Rev Gastroenterol Hepatol, 2012. **9**(8): p. 454-67.
87. Kraman, M., et al., *Suppression of antitumor immunity by stromal cells expressing fibroblast activation protein-alpha.* Science, 2010. **330**(6005): p. 827-30.
88. Ene-Obong, A., et al., *Activated pancreatic stellate cells sequester CD8+ T cells to reduce their infiltration of the juxtatumoral compartment of pancreatic ductal adenocarcinoma.* Gastroenterology, 2013. **145**(5): p. 1121-32.
89. Tjomsland, V., et al., *The desmoplastic stroma plays an essential role in the accumulation and modulation of infiltrated immune cells in pancreatic adenocarcinoma.* Clin Dev Immunol, 2011. **2011**: p. 212810.

90. Erkan, M., et al., *The activated stroma index is a novel and independent prognostic marker in pancreatic ductal adenocarcinoma.* Clin Gastroenterol Hepatol, 2008. **6**(10): p. 1155-61.
91. Kroemer, G. and J. Pouyssegur, *Tumor cell metabolism: cancer's Achilles' heel.* Cancer Cell, 2008. **13**(6): p. 472-82.
92. Martinez-Outschoorn, U.E., et al., *Cancer metabolism: a therapeutic perspective.* Nat Rev Clin Oncol, 2017. **14**(1): p. 11-31.
93. Kelderman, S., et al., *Lactate dehydrogenase as a selection criterion for ipilimumab treatment in metastatic melanoma.* Cancer Immunol Immunother, 2014. **63**(5): p. 449-58.
94. Pearce, E.L. and E.J. Pearce, *Metabolic pathways in immune cell activation and quiescence.* Immunity, 2013. **38**(4): p. 633-43.
95. Ward, P.S. and C.B. Thompson, *Metabolic reprogramming: a cancer hallmark even warburg did not anticipate.* Cancer Cell, 2012. **21**(3): p. 297-308.
96. Warburg, O., *On respiratory impairment in cancer cells.* Science, 1956. **124**(3215): p. 269-70.
97. Pfeiffer, T., S. Schuster, and S. Bonhoeffer, *Cooperation and competition in the evolution of ATP-producing pathways.* Science, 2001. **292**(5516): p. 504-7.
98. Vander Heiden, M.G., L.C. Cantley, and C.B. Thompson, *Understanding the Warburg effect: the metabolic requirements of cell proliferation.* Science, 2009. **324**(5930): p. 1029-33.
99. Wang, R. and D.R. Green, *Metabolic checkpoints in activated T cells.* Nat Immunol, 2012. **13**(10): p. 907-15.
100. Rafalski, V.A., E. Mancini, and A. Brunet, *Energy metabolism and energy-sensing pathways in mammalian embryonic and adult stem cell fate.* J Cell Sci, 2012. **125**(Pt 23): p. 5597-608.
101. Harvey, A.J., K.L. Kind, and J.G. Thompson, *REDOX regulation of early embryo development.* Reproduction, 2002. **123**(4): p. 479-86.
102. O'Neill, L.A., R.J. Kishton, and J. Rathmell, *A guide to immunometabolism for immunologists.* Nat Rev Immunol, 2016. **16**(9): p. 553-65.
103. Chang, C.H., et al., *Metabolic Competition in the Tumor Microenvironment Is a Driver of Cancer Progression.* Cell, 2015. **162**(6): p. 1229-41.
104. Russo, V. and M.P. Protti, *Tumor-derived factors affecting immune cells.* Cytokine Growth Factor Rev, 2017. **36**: p. 79-87.
105. Molon, B., B. Cali, and A. Viola, *T Cells and Cancer: How Metabolism Shapes Immunity.* Front Immunol, 2016. **7**: p. 20.
106. Corrado, M., L. Scorrano, and S. Campello, *Changing perspective on oncometabolites: from metabolic signature of cancer to tumorigenic and immunosuppressive agents.* Oncotarget, 2016. **7**(29): p. 46692-46706.
107. Renner, K., et al., *Metabolic Hallmarks of Tumor and Immune Cells in the Tumor Microenvironment.* Front Immunol, 2017. **8**: p. 248.
108. Calcinotto, A., et al., *Modulation of microenvironment acidity reverses anergy in human and murine tumor-infiltrating T lymphocytes.* Cancer Res, 2012. **72**(11): p. 2746-56.
109. Vander Heiden, M.G. and R.J. DeBerardinis, *Understanding the Intersections between Metabolism and Cancer Biology.* Cell, 2017. **168**(4): p. 657-669.
110. Vander Heiden, M.G., *Targeting cancer metabolism: a therapeutic window opens.* Nat Rev Drug Discov, 2011. **10**(9): p. 671-84.
111. Galluzzi, L., et al., *Metabolic targets for cancer therapy.* Nat Rev Drug Discov, 2013. **12**(11): p. 829-46.
112. Marchiq, I. and J. Pouyssegur, *Hypoxia, cancer metabolism and the therapeutic benefit of targeting lactate/H(+) symporters.* J Mol Med (Berl), 2016. **94**(2): p. 155-71.

113. Melero, I., et al., *Evolving synergistic combinations of targeted immunotherapies to combat cancer.* Nat Rev Cancer, 2015. **15**(8): p. 457-72.
114. Sukumar, M., R.J. Kishton, and N.P. Restifo, *Metabolic reprograming of anti-tumor immunity.* Curr Opin Immunol, 2017. **46**: p. 14-22.
115. Pearce, E.L., et al., *Enhancing CD8 T-cell memory by modulating fatty acid metabolism.* Nature, 2009. **460**(7251): p. 103-7.
116. Michalek, R.D., et al., *Cutting edge: distinct glycolytic and lipid oxidative metabolic programs are essential for effector and regulatory CD4+ T cell subsets.* J Immunol, 2011. **186**(6): p. 3299-303.
117. Klebanoff, C.A., et al., *Central memory self/tumor-reactive CD8+ T cells confer superior antitumor immunity compared with effector memory T cells.* Proc Natl Acad Sci U S A, 2005. **102**(27): p. 9571-6.
118. Gattinoni, L., et al., *Wnt signaling arrests effector T cell differentiation and generates CD8+ memory stem cells.* Nat Med, 2009. **15**(7): p. 808-13.
119. Zanon, V., et al., *Curtailed T-cell activation curbs effector differentiation and generates CD8(+) T cells with a naturally-occurring memory stem cell phenotype.* Eur J Immunol, 2017. **47**(9): p. 1468-1476.
120. Lugli, E., et al., *Identification, isolation and in vitro expansion of human and nonhuman primate T stem cell memory cells.* Nat Protoc, 2013. **8**(1): p. 33-42.
121. Gattinoni, L., et al., *A human memory T cell subset with stem cell-like properties.* Nat Med, 2011. **17**(10): p. 1290-7.
122. Cieri, N., et al., *IL-7 and IL-15 instruct the generation of human memory stem T cells from naive precursors.* Blood, 2013. **121**(4): p. 573-84.
123. Sukumar, M., et al., *Inhibiting glycolytic metabolism enhances CD8+ T cell memory and antitumor function.* J Clin Invest, 2013. **123**(10): p. 4479-88.
124. Cappello, P., et al., *Vaccination with ENO1 DNA prolongs survival of genetically engineered mice with pancreatic cancer.* Gastroenterology, 2013. **144**(5): p. 1098-106.
125. Altman, D.G., et al., *Reporting recommendations for tumor marker prognostic studies (REMARK): explanation and elaboration.* BMC Med, 2012. **10**: p. 51.
126. Siegel, R.L., K.D. Miller, and A. Jemal, *Cancer Statistics, 2017.* CA Cancer J Clin, 2017. **67**(1): p. 7-30.
127. Di Caro, G., et al., *Occurrence of tertiary lymphoid tissue is associated with T-cell infiltration and predicts better prognosis in early-stage colorectal cancers.* Clin Cancer Res, 2014. **20**(8): p. 2147-58.
128. de Visser, K.E., L.V. Korets, and L.M. Coussens, *De novo carcinogenesis promoted by chronic inflammation is B lymphocyte dependent.* Cancer Cell, 2005. **7**(5): p. 411-23.
129. Kroeger, D.R., K. Milne, and B.H. Nelson, *Tumor-Infiltrating Plasma Cells Are Associated with Tertiary Lymphoid Structures, Cytolytic T-Cell Responses, and Superior Prognosis in Ovarian Cancer.* Clin Cancer Res, 2016. **22**(12): p. 3005-15.
130. Thaunat, O., et al., *B cell survival in intragraft tertiary lymphoid organs after rituximab therapy.* Transplantation, 2008. **85**(11): p. 1648-53.
131. Martin, F. and A.C. Chan, *B cell immunobiology in disease: evolving concepts from the clinic.* Annu Rev Immunol, 2006. **24**: p. 467-96.
132. Gunderson, A.J. and L.M. Coussens, *B cells and their mediators as targets for therapy in solid tumors.* Exp Cell Res, 2013. **319**(11): p. 1644-9.
133. Barbera-Guillem, E., et al., *B lymphocyte pathology in human colorectal cancer. Experimental and clinical therapeutic effects of partial B cell depletion.* Cancer Immunol Immunother, 2000. **48**(10): p. 541-9.
134. Aklilu, M., et al., *Depletion of normal B cells with rituximab as an adjunct to IL-2 therapy for renal cell carcinoma and melanoma.* Ann Oncol, 2004. **15**(7): p. 1109-14.

135. Affara, N.I., et al., *B cells regulate macrophage phenotype and response to chemotherapy in squamous carcinomas.* Cancer Cell, 2014. **25**(6): p. 809-821.
136. Zhang, Y., et al., *B cell regulation of anti-tumor immune response.* Immunol Res, 2013. **57**(1-3): p. 115-24.
137. Zhang, Y., et al., *B lymphocyte inhibition of anti-tumor response depends on expansion of Treg but is independent of B-cell IL-10 secretion.* Cancer Immunol Immunother, 2013. **62**(1): p. 87-99.
138. Shah, S., et al., *Increased rejection of primary tumors in mice lacking B cells: inhibition of anti-tumor CTL and TH1 cytokine responses by B cells.* Int J Cancer, 2005. **117**(4): p. 574-86.
139. Qin, Z., et al., *B cells inhibit induction of T cell-dependent tumor immunity.* Nat Med, 1998. **4**(5): p. 627-30.
140. Perricone, M.A., et al., *Enhanced efficacy of melanoma vaccines in the absence of B lymphocytes.* J Immunother, 2004. **27**(4): p. 273-81.
141. Inoue, S., et al., *Inhibitory effects of B cells on antitumor immunity.* Cancer Res, 2006. **66**(15): p. 7741-7.
142. Kim, S., et al., *B-cell depletion using an anti-CD20 antibody augments antitumor immune responses and immunotherapy in nonhematopoetic murine tumor models.* J Immunother, 2008. **31**(5): p. 446-57.
143. Forte, G., et al., *Inhibition of CD73 improves B cell-mediated anti-tumor immunity in a mouse model of melanoma.* J Immunol, 2012. **189**(5): p. 2226-33.
144. DiLillo, D.J., K. Yanaba, and T.F. Tedder, *B cells are required for optimal CD4+ and CD8+ T cell tumor immunity: therapeutic B cell depletion enhances B16 melanoma growth in mice.* J Immunol, 2010. **184**(7): p. 4006-16.
145. Pollizzi, K.N. and J.D. Powell, *Integrating canonical and metabolic signalling programmes in the regulation of T cell responses.* Nat Rev Immunol, 2014. **14**(7): p. 435-46.
146. MacIver, N.J., R.D. Michalek, and J.C. Rathmell, *Metabolic regulation of T lymphocytes.* Annu Rev Immunol, 2013. **31**: p. 259-83.
147. Fox, C.J., P.S. Hammerman, and C.B. Thompson, *Fuel feeds function: energy metabolism and the T-cell response.* Nat Rev Immunol, 2005. **5**(11): p. 844-52.
148. Norata, G.D., et al., *The Cellular and Molecular Basis of Translational Immunometabolism.* Immunity, 2015. **43**(3): p. 421-34.
149. Feig, C., et al., *Targeting CXCL12 from FAP-expressing carcinoma-associated fibroblasts synergizes with anti-PD-L1 immunotherapy in pancreatic cancer.* Proc Natl Acad Sci U S A, 2013. **110**(50): p. 20212-7.
150. Beatty, G.L., et al., *Exclusion of T Cells From Pancreatic Carcinomas in Mice Is Regulated by Ly6C(low) F4/80(+) Extratumoral Macrophages.* Gastroenterology, 2015. **149**(1): p. 201-10.
151. Yu, J., et al., *Digital next-generation sequencing identifies low-abundance mutations in pancreatic juice samples collected from the duodenum of patients with pancreatic cancer and intraductal papillary mucinous neoplasms.* Gut, 2017. **66**(9): p. 1677-1687.
152. Hart, C.D., et al., *Serum Metabolomic Profiles Identify ER-Positive Early Breast Cancer Patients at Increased Risk of Disease Recurrence in a Multicenter Population.* Clin Cancer Res, 2017. **23**(6): p. 1422-1431.
153. Takis, P.G., et al., *(1)H-NMR based metabolomics study for the detection of the human urine metabolic profile effects of Origanum dictamnus tea ingestion.* Food Funct, 2016. **7**(9): p. 4104-15.
154. Bathe, O.F., et al., *Feasibility of identifying pancreatic cancer based on serum metabolomics.* Cancer Epidemiol Biomarkers Prev, 2011. **20**(1): p. 140-7.

155. Napoli, C., et al., *Urine metabolic signature of pancreatic ductal adenocarcinoma by (1)h nuclear magnetic resonance: identification, mapping, and evolution.* J Proteome Res, 2012. **11**(2): p. 1274-83.
156. Sugimoto, M., et al., *Capillary electrophoresis mass spectrometry-based saliva metabolomics identified oral, breast and pancreatic cancer-specific profiles.* Metabolomics, 2010. **6**(1): p. 78-95.
157. Zamarin, D., et al., *Localized oncolytic virotherapy overcomes systemic tumor resistance to immune checkpoint blockade immunotherapy.* Sci Transl Med, 2014. **6**(226): p. 226ra32.
158. Taube, J.M., et al., *Colocalization of inflammatory response with B7-h1 expression in human melanocytic lesions supports an adaptive resistance mechanism of immune escape.* Sci Transl Med, 2012. **4**(127): p. 127ra37.
159. Weide, B., et al., *Baseline Biomarkers for Outcome of Melanoma Patients Treated with Pembrolizumab.* Clin Cancer Res, 2016. **22**(22): p. 5487-5496.
160. Martens, A., et al., *Baseline Peripheral Blood Biomarkers Associated with Clinical Outcome of Advanced Melanoma Patients Treated with Ipilimumab.* Clin Cancer Res, 2016. **22**(12): p. 2908-18.
161. Haas, R., et al., *Lactate Regulates Metabolic and Pro-inflammatory Circuits in Control of T Cell Migration and Effector Functions.* PLoS Biol, 2015. **13**(7): p. e1002202.
162. Fischer, K., et al., *Inhibitory effect of tumor cell-derived lactic acid on human T cells.* Blood, 2007. **109**(9): p. 3812-9.
163. Brand, A., et al., *LDHA-Associated Lactic Acid Production Blunts Tumor Immunosurveillance by T and NK Cells.* Cell Metab, 2016. **24**(5): p. 657-671.
164. Wherry, E.J., et al., *Molecular signature of CD8+ T cell exhaustion during chronic viral infection.* Immunity, 2007. **27**(4): p. 670-84.
165. Schietinger, A. and P.D. Greenberg, *Tolerance and exhaustion: defining mechanisms of T cell dysfunction.* Trends Immunol, 2014. **35**(2): p. 51-60.
166. Patsoukis, N., et al., *PD-1 alters T-cell metabolic reprogramming by inhibiting glycolysis and promoting lipolysis and fatty acid oxidation.* Nat Commun, 2015. **6**: p. 6692.
167. Badoual, C., et al., *PD-1-expressing tumor-infiltrating T cells are a favorable prognostic biomarker in HPV-associated head and neck cancer.* Cancer Res, 2013. **73**(1): p. 128-38.
168. Sauce, D., et al., *PD-1 expression on human CD8 T cells depends on both state of differentiation and activation status.* AIDS, 2007. **21**(15): p. 2005-13.